Performance Analysis and Resource Allocations for a WPCN with a New Nonlinear Energy Harvester Model

Danyang Wang, Fatemeh Rezaei, *Student Member, IEEE,* and Chintha Tellambura, *Fellow, IEEE*

Wireless powered communication networks (WPCNs) are commonly analyzed by using the linear energy harvesting (EH) model. However, since practical EH circuits are non-linear, the use of the linear EH model gives rise to distortions and mismatches. To overcome these issues, we propose a more realistic, nonlinear EH model. The model is based upon the error function and has three parameters. Their values are determined to best fit with measured data. We also develop the asymptotic version of this model. For comparative evaluations, we consider the linear and rational EH models. With these four EH models, we investigate the performance of a WPCN. It contains a multiple-antenna power station (PS), a signal-antenna wireless device (WD), and a multiple-antenna information receiving station (IRS). The WD harvests the energy broadcast by the PS in the PS-WD link, and then it uses the energy in the WD-IRS link to transfer information. We analyze the average throughput of delay-limited and delay-tolerant transmission modes as well as the average bit error rate (BER) of binary phase-shift keying (BPSK) and binary differential phase-shift keying (BDPSK) over the four EH modes. As well, we derive the asymptotic expressions for the large PS antenna case and the effects of transmit power control. Furthermore, for the case of multiple WDs, we optimize energy beamforming and time allocation to maximize the minimum rate of the WDs. Finally, the performances of four EH models are validated by Monte-Carlo simulations.

Index Terms—nonlinear energy harvesting, wireless powered communications network, average throughput, bit error rate, resource allocation.

I. INTRODUCTION

A. Background and Motivation

Internet of Things (IoT) is a network to connect people, processes, data, and things. Globally, IoT connections will grow 2.4-fold, from 6.1 billion in 2018 to 14.7 billion by 2023 [1]. Mixed devices and connections are enabling myriad IoT apps. Connected-home, video-surveillance, connected appliances, and tracking apps will make up 48% of IoT connections by 2023. In the fifth-generation (5G) wireless, massive machine type communication (mMTC) enables tens of billions of low-complexity, low-power devices to connect [2]. Thus, charging or replacing their batteries regularly adds to the cost and complexity of the networks. Thus, energy harvesting is an attractive option [3]. For example, the commercial energy transmitters and radio frequency (RF) energy harvesters have been developed by Powercast [4]. On the other hand, harvesting energy from RF signals can be up to a few kilometers [5]. Ambient RF signals are ubiquitous from cellular base stations, television stations, wireless routers and others. Alternatively, dedicated RF power transmitters may also be deployed [5].

These advantages have led to the harvest-then-transmit protocol [6] and wireless powered communications networks (WPCNs). That is, a power station (PS) or hybrid AP transfers energy to a wireless user in the downlink, who harvests energy and transmits information in the uplink to the data receiver. The resulting energy harvesting (EH) paradigm has been heavily researched [7]–[11]. While many works focus on the EH performance for various wireless applications, the characteristics of the EH circuit are a fundamental issue [12], [13]. Since these characteristics in fact determine the amount of harvested energy [14], several EH models have been developed.

B. Energy Harvester Models and Resource Allocations

The linear EH model is the de facto standard for most works [6], [8], [10], [15]–[18]. It assumes that the output power of the energy harvester increases linearly with the input RF signal power. It thus suffers from two limitations. First, empirical works [19]–[22] demonstrate that practical EH circuits display nonlinear characteristics, exhibiting a saturation plateau with high input powers. This fact directly follows from the fact that EH circuits employ nonlinear elements such as diodes and transistors [21], [23]. Thus, the unbounded increase predicted by the linear model is empirically wrong [24], [25]. Second, the output of the EH circuit drops to zero if the input RF is below a minimum input power level, which is known as the sensitivity level of the circuit. For example, it is $-25\,\text{dBm}$ at $1.3\,\text{GHz}$ for an EH circuit of 130-nm CMOS (complementary metal-oxide-semiconductor) [13] and $-22\,\text{dBm}$ at $915\,\text{MHz}$ for a 180-nm CMOS [26]. Most energy harvesters have an activation level due to the diode turn-on voltage, and if the received energy is below the level, the input energy is too small to be harvested [27]. Clearly, these two key properties of practical EH circuits are not correctly represented by the standard linear EH model.

Thus, to represent practical EH circuits more accurately, several nonlinear models have been developed. Specifically, they include a piece-wise linear function [28], a rational function [29], a polynomial function [30], a sigmoid function [31], or an improved sigmoid function [32]. We briefly discuss their applications next.

Although the model [28] captures the saturation effect of practical EH circuits, it assumes a linear response up to

D. Wang, F. Rezaei and C. Tellambura are with the Department of Electrical and Computer Engineering, University of Alberta, Edmonton, Canada (e-mail: {danyang5, rezaeidi, ct4}@ualberta.ca).

the saturation level. Thus, this model may not fully match measured data. Nevertheless, this model offers a degree of analytical tractability and has thus been employed for outage performance analysis of relays [33], [34], secrecy analysis of relays [35], throughput analysis of WPCNs [36], and resource allocation of a WPCN [24]. Since the rational EH model [29] is not analytically tractable, it has been modified to a simpler form [14]. Both the models correctly exhibit the saturation characteristic. The polynomial model is obtained by truncating the Taylor expansion of the diode output and it has been used for signal optimization [30]. The sigmoid model posits a logistic transfer function between the input and output powers [31]. It captures the saturation characteristic of practical circuits but assumes zero sensitivity. It has been used to study resource allocation for non-orthogonal multiple access (NOMA) cognitive radio networks in [37], [38], outage probability and throughput [39] and many more. The sigmoid model has been modified in [32] to incorporate non-zero sensitivity levels. This modified model has been applied for energy beamforming optimization [40]. The non-linear models of [31] and [32] have been studied in [41]. We hasten to add that this overview is by no means complete.

Resource allocations have been extensively investigated for EH systems [6], [8], [10], [16], [31], [37], [41]. However, some of them consider the simple linear EH model, for which the resource allocation problems are relatively easy to solve [6], [8], [10], [16]. Resource allocation schemes highly depend on accurate mathematical models for the RF EH circuits and the discrepancy between the properties of practical nonlinear EH circuits and the linear EH model may cause performance degradation in practical implementation due to the drastic resource allocation mismatches [42]. There are a few papers investigating resource allocations for WPCNs with nonlinear EH models [24], [40], [42]. In particular, in [42], with the sigmoid nonlinear EH model, the time allocation and power control of a multi-user WPCN system are jointly optimized to maximize the minimum individual throughput. In this scheme, the uplink WDT is supported through time division multiple access (TDMA) with multi-input multi-output (MIMO) transceivers. The authors in [24] also investigate the optimal time and power allocation of a multi-user TDMA WPCN With the peice-wise linear EH model. Moreover, reference [40] adopts the sigmoid nonlinear EH model with sensitivity and investigates the energy beamforming and time allocation problem to maximize the rate fairness. In this scheme, the hybrid AP supports WPT via energy beamforming and WDT via space-division-multiple-access (SDMA).

C. Problem Statement and Contributions

The above review makes it clear that the non-linearity of practical EH circuits will clearly affect the performance and design of WPCNs and that the mismatch between the linear EH model and measured data can lead to bad design choices. For example, performance analysis based upon the linear model predicts overoptimistic results in terms of the common performance measures such as outage, ergodic capacity, error rate and so on. Additionally, the use of the linear EH model

could be misleading for the uplink sum rate maximization problems. For these reasons, we need more accurate EH models.

In this paper, we first propose two new nonlinear EH models. The first model has four parameters, which can be determined via a best-fit search of measured data [22], [23], [43]. The second is a simplified version of the first. We also develop a detailed performance analysis and investigated a resource allocation for a WPCN.

The main contributions are summarized as follows:

1) We suggest a new nonlinear EH model (NLEH), based on the error function. This model consists of four parameters, which can be estimated by simple best-fit search with measured data. We also develop a new, simplified asymptotic model (AM). These two are then compared against the standard linear model (LM) and the rational model (RM) due to [14].

2) To comparatively evaluate these four models, we investigate the throughput of the WPCN (Fig. 3) and bit error rates (BER) of binary phase-shift keying (BPSK), binary differential phase-shift keying (BDPSK) modulations. In particular, we derive the throughput of delay limited or tolerant modes.

3) We also consider the large antenna regime at the power station. In this case, the received power at the wireless device tends to the normal distribution. By exploiting this fact, we find the asymptotic throughput and BER expressions for new the EH model. Asymptotic results of other models can be derived similarly. The impact of transmit power control is also analyzed.

4) Optimal energy beamforming and time allocation are developed with the proposed EH models for multiple wireless devices (WDs). In particular, we maximize the rate fairness across them. We show that the optimal energy beamformer significantly outperforms omnidirectional beamforming.

Furthermore, we assess the impact of the transmit power of the power station, the EH time, power amplifier efficiency at WD, the number of PS antennas and the number of IRS antennas via numerical simulations. From numerical results, we show that NLEH, AM, and RM models accurately reach the saturation state of practical EH circuits, but the LM model does not.

Notation: For random variable (RV) X, $f_X(\cdot)$ and $F_X(\cdot)$ denote the probability density function (PDF) and cumulative distribution function (CDF). A circularly symmetric complex Gaussian vector with mean μ and correlation matrix $\mathbf{B}$ is $\mathcal{CN}(\mu, \mathbf{B})$. The gamma function $\Gamma(a)$ is given in [44, Eq. (8.310.1)]; $\Gamma(a, x)$ is upper incomplete Gamma function given in [44, Eq. (8.350.2)]; $\Psi(a, b; z)$ is the confluent hypergeometric function [44, Eq. (9.211.4)]; $\gamma(n, x)$ is the lower incomplete gamma function [44, Eq. (8.350)]; $K_\nu(\cdot)$ is the ν-th order modified Bessel function of the second kind [44, Eq. (8.432)]; $G_{pq}^{mn}\left(z \mid \begin{smallmatrix} a_1 \cdots a_p \\ b_1 \cdots b_q \end{smallmatrix}\right)$ denotes the Meijer G-function [44, Eq. (9.301)].

This paper is organized as follows. In Section II, we describe the new nonlinear EH model, its asymptotic version, the standard linear EH model and the rational EH model.

In Section III, we introduce the system model. Section IV analyzes the average throughput of delay-limited and delay-tolerant transmission modes as well as the average BER of BPSK and BDPSK for four EH models. Large antenna case and transmit power control are also considered in this section. In Section V, the resource allocation with four EH models are described. Section VI studies energy beamforming optimization. In Section VII, numerical results show the accuracy of the exact and asymptotic results. Sections VIII provides the concluding remarks. Finally, some derivations are relegated to the appendices.

II. EH MODELS

A. New Energy Harvesting Model

As mentioned in Section I-B, there are two limitations in the practical EH circuits: First, for large input powers, the output power exhibits a saturation plateau. Second, when the input power is lower than the sensitivity level, the output is zero. Here, we suggest a nonlinear EH model that captures the saturation and sensitivity character of practical circuits. The model posits that the harvested power at the output of the EH circuit can be expressed as

$$P_h = P_{\max} \left[\frac{\text{erf}(a((P_r - P_{se}) + b)) - \text{erf}(ab)}{1 - \text{erf}(ab)} \right]^+ \triangleq q(P_r),$$
(1)

where $P_{\max}$ is the maximum harvested power level, and P_r is the received RF power input, $a > 0$ and $b > 0$ are two parameters, P_{se} is the input sensitivity level such that that output power falls to zero if $P_r \leq P_{se}$, and $[x]^+ = \max(x, 0)$. And $\text{erf}(x) = \frac{2}{\sqrt{\pi}} \int_0^x e^{-t^2} dt$ is the well-known error function.

The intuition for this model comes from the following observation. Since practical EH circuits exhibit a saturation region for large input powers, this behavior must be modeled by a smooth function. The error function is suitable for this purpose because for large x, $\text{erf}(x)$ tends to one; thus, in (1), as P_r gets large, the harvested power P_h converges to $P_{\max}$. Of course, $\text{erf}(x)$ is not the only such function. The parameters a, b and $P_{\max}$ can be determined via a best-fit match with experimental data.

The model (1) is general enough for a wide variety of applications. However, perhaps the simplest way to compare it against others is to compute the average of P_h. This depends on fading and other details of the EH link. In this paper, we consider a specific WPCN (Fig. 3), which consists of a PS with $N \geq 1$ antennas and a wireless device (WD), which harvests RF energy. Suppose that the PS transmits at power level P_t. Let the large-scale path-loss between PS and WD be Ω_1 and the small-scale channel be $\mathbf{h}$. Further details of these can be found in Section III. The received RF signal power with maximum ratio transmission (MRT) beamforming at the PS, i.e., $\mathbf{w} = \frac{\mathbf{h}}{||\mathbf{h}||}$ [45], becomes $P_r = P_t \Omega_1 ||\mathbf{h}||^2 G_{\text{PS}} G_{\text{WD}} = \bar{P}_t ||\mathbf{h}||^2$ where G_{PS} and G_{WD} are the antenna gains of PS and WD, and $\bar{P}_t = P_t \Omega_1 G_{\text{PS}} G_{\text{WD}}$ is the transmit power corrected by the antenna gains and the path-loss. Thus, assuming the distance

remains fixed, the average harvested power by the WD under this EH model is given by

$$\mathbb{E}[P_h] = \int_{P_{se}}^{\infty} q(x) f_{P_r}(x) dx$$
(2)

where $f_{P_r}(x)$ is the PDF of the received power, which is given as (see Section III)

$$f_{P_r}(x) = \frac{1}{\left(\bar{P}_t\right)^N \Gamma(N)} x^{N-1} e^{-\frac{x}{\bar{P}_t}}, \quad 0 \leq x < \infty.$$
(3)

However, we need a comparative evaluation for a better assessment of the impact of different EH models. Thus, we consider the following three models.

B. Asymptotic Model

To find a simpler model, we consider the region where the input RF power to the EH circuit is large. This can happen when the transmit power of the PS grows large and the channel fading is negligible. The new nonlinear model (1) then predicts that the harvested power level will be $P_{\max}$. Based on this fact, we suggest the following simple asymptotic model:

$$P_a = P_{\max} \left[1 - e^{-\kappa(P_r - P_{se})} \right]^+ \triangleq q_{as}(P_r),$$
(4)

where κ is a constant. It can be seen that, as per Fig. 1 and Table I, the asymptotic model is good for P_r as small as $500\mu W$. This model is simpler than (1) and may be more analytically tractable. Clearly, this model is very consistent with (1) in the asymptotic region. But we can choose κ to make this model as accurate as possible for the entire input power range. While there may be several ways to find an optimal value of κ, a simple option is to make sure that both (1) and (4) have the same gradient at the input zero ($P_r = P_{se}$). Thus, by matching the first derivatives of (1) and (4) at $P_r = P_{se}$ point, we find

$$\kappa = 2 \frac{e^{-a^2 b^2} a}{\sqrt{\pi} (1 - \text{erf}(ab))}.$$

To recap, once we have measured data, the parameters of both of these models, (1) and (4), can be estimated readily.

As before, for comparative evaluations, we must compute the average of P_{se}. We consider the same WPCN (Fig. 3). With the same details given before, the average harvested power at the WD is given by

$$\mathbb{E}[P_a] = \int_{P_{se}}^{\infty} q_{as}(x) f_{P_r}(x) dx$$
$$= \frac{P_{\max}}{\bar{P}_t^N \Gamma(N)} \int_{P_{se}}^{\infty} (1 - e^{-\kappa(x - P_{se})}) x^{N-1} e^{-\frac{x}{\bar{P}_t}} dx$$
$$= \frac{P_{\max}}{\Gamma(N)} \left[\Gamma\left(N, \frac{P_{se}}{\bar{P}_t}\right) - \frac{e^{\kappa P_{se}} \Gamma\left(N, P_{se}\left(\kappa + \frac{1}{\bar{P}_t}\right)\right)}{\left(1 + \kappa \bar{P}_t\right)^N} \right],$$
(5)

where $\Gamma(a, x)$ is upper incomplete Gamma function given in [44, Eq. (8.350.2)] and the integral is obtained from [44, Eq. (3.351.3)].

C. Linear Model

For completeness and for comparative evaluation purposes, we also consider the linear EH model, the most commonly used one in the literature. According to this model, the harvested power at the output of the EH circuit is given by

$$P_l = \mu(P_r - P_{se})^+ \triangleq q_l(P_r). \qquad (6)$$

This model has only one parameter, namely μ. It can be found by curve fitting with the measured input-output data of practical EH circuits.

However, in this case, we must compare this model with our NLEH model (1). To do so, we simply match the gradient of (1) at input $P_r = P_{se}$ with the constant μ. Thus it is given by

$$\mu = 2P_{\max} \frac{e^{-a^2 b^2} a}{\sqrt{\pi}\left(1 - \mathrm{erf}\left(ab\right)\right)}.$$

Once again, this constant is derived by matching the first derivatives of (1) and (6) at $P_r = P_{se}$ point.

As before, we would like to compute the average of P_l. We consider the specific WPCN (Fig. 3). With the same details given before, the average harvested power at the WD is given by

$$\begin{aligned}
\mathbb{E}[P_l] &= \mu E[P_r] \\
&= \frac{\mu}{\bar{P}_t^N \Gamma(N)} \int_{P_{se}}^{\infty} (x - P_{se}) x^{N-1} e^{-\frac{x}{\bar{P}_t}} dx \qquad (7) \\
&= \frac{\mu \bar{P}_t}{\Gamma(N)} \Gamma\left(N+1, \frac{P_{se}}{\bar{P}_t}\right) - \frac{\mu P_{se}}{\Gamma(N)} \Gamma\left(N, \frac{P_{se}}{\bar{P}_t}\right),
\end{aligned}$$

where integral is obtained from [44, Eq. (3.351.3)] and $\Gamma(a, x)$ is the incomplete gamma function. Unsurprisingly, this models predicts a linear increase of the average harvested power with the transmit power. This however does not match with the behaviour of practical EH circuits.

D. Rational Model

Rational models express the output power of the EH circuit as a ratio of two polynomials. For example, [29] examines a large number of energy harvesters and develops a detailed rational model. But this model ends up with seven parameters. Thus, a simplified version proposed in [14], which is equivalent to the following:

$$P_{rat} = P_{\max} \left[\frac{P_r - P_{se}}{P_r + \beta}\right]^+ \triangleq q_{rat}(P_r). \qquad (8)$$

This model has only two parameters, namely $P_{\max}$ and β. They can be found by best-fit search with the measured data.

However, in this case, we want to compare this model with our NLEH model (1). To do so, constant β is derived by matching the first derivatives of (1) and (8) at $P_r = P_{se}$ point. Thus, we find

$$\beta = \frac{\sqrt{\pi}\left(1 - \mathrm{erf}\left(ab\right)\right)}{2e^{-a^2 b^2} a}.$$

As before, we would like to compute the average of P_{rat}. We consider the specific WPCN (Fig. 3). With the same details given before, Under this model, the average harvested power at the WD is given by

$$\mathbb{E}[P_{rat}] = \int_{P_{se}}^{\infty} q_{rat}(x) f_{P_r}(x) dx. \qquad (9)$$

TABLE I
MODEL COMPARISON

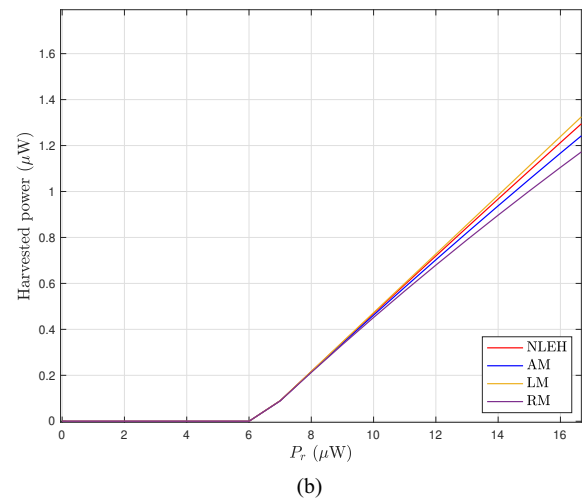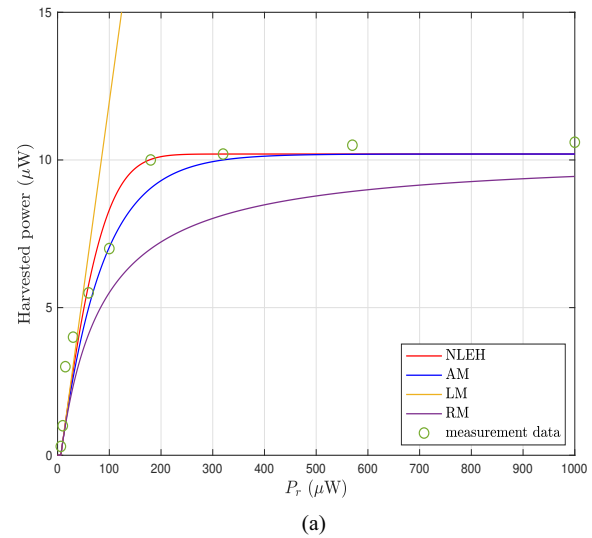| Model	NLEH	[40]	[28]	AM	RM	LM
RMSE	0.86	0.95	1.30	0.87	1.69	42.88
Parameters	4	4	3	3	3	2
Accuracy	high	high	good	high	good	poor
Tractability	low	low	good	good	good	best

E. Model comparisons

(a)

(b)

Fig. 1. Input-output relationship of the models: (a) in the overall region; (b) in the sensitivity region [21]. The measurement data is obtained from [21, Fig. (17.d)].

The parameters of the piece-wise model, the sigmoid model, and the NLEH model are all obtained via the built-in genetic algorithm of Matlab. To determine the parameter values of each model, this algorithm minimizes the mean square error between the model and the measured data.

To illustrate this process, we first the parameters of the proposed new NLEH (1) by using the measurement data

given in [21, Fig. (17.d)]. This paper gives P_{se} to be -22 dBm. We use this value in (1) and find the three remaining NLEH parameters as $a = 0.0088$, $b = 25.6410\,\mu\text{W}$ and $P_{\max} = 10.2010\,\mu\text{W}$ with a root mean square error (RMSE) of 0.8591. The same process is applied to the other models as well. Fig. 1 (a) depicts the match between these models and the measured data. Fig. 1 (b) plots the sensitivity region with P_{se} being $-22\,\text{dBm}$ ($6.3\,\mu\text{W}$). It can be seen when the input power is less than the sensitivity level, the output power is 0. In Table I, we compared the RMSE values for several models. It is interesting to note that both AM and RM models achieve fairly small RMSE deviations. In contrast, the linear model has an extremely poor fit with the measured data (e.g., the extremely large RMSE value). Thus, we may expect that the use of the LM model will be overly optimistic compared to the other three models.

On the other hand, the LM model may be improved by adding a saturation effect. This gives rise to the so-called piece-wise linear model It has a knee point, which is the main parameter. The knee point is determined to best fit the measured data. We use the built-in genetic algorithm of Matlab to find this parameter by minimizing the RMSE. The RMSE in this case is found to be 1.30. So this model does much better than the linear model (RMSE is 42.88). Thus, we see that our proposed NLEH and AM models achieve better accuracy than the piece-wise linear model [28].

Compared with the sigmoid model with sensitivity of [40], we see that our proposed NLEH model is a bit more accurate in terms of the RMSE. We have observed the same situation with another data set in [23, Fig. (5)]. This limited comparison based on [21], [23] suggests that the new NLEH model provides a better approximation to the measured data than the other EH models. Of course, this situation may reverse for other measured data. Table I also includes a comparison of several qualitative measures. For example, in terms of analytical tractability, the linear model is the best, which is why it is the most commonly used model. In some case, the linear models also enables the development of closed-form solutions.

Fig. 2 compares the four models, (1), (4), (6) and (8) in terms of the average harvested power at the WD. We assume the EH circuit is part of the WD in the communication system (Fig. 3). The PS has $N = 3$ antennas and the WD has one. All the three nonlinear EH models show the saturation plateau, which coincides with measured data in Fig. 1. Clearly, RM and AM models approximate the NLEH model well for high input powers. However, the LM is inaccurate in modelling of practical EH circuits as the transmit power increases. Despite that, it can approximate the practical EH circuit for low transmit powers (< -18 dBm). Overall, the use of the LM model yields optimistic upper bounds on performance.

These four EH models will next be used for a system performance analysis. To set the scene for that, we next describe the communication system model.

For the rest of the paper, we assume $P_{se} = 0$. This enables some closed-form analysis as well as compact performance expressions.
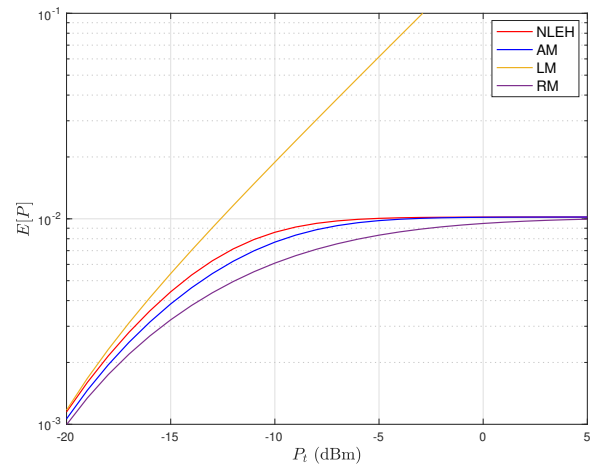

Fig. 2. $E[P]$ of four EH models versus P_t (dBm). Parameters $a = 0.0088$, $b = 25.6410\,\mu\text{W}$ and $P_{\max} = 10.2010\,\mu\text{W}$, $N = 3$, $G_{\text{PS}} = 11\,\text{dBi}$, $G_{\text{WD}} = 3\,\text{dBi}$, and the distance between PS and WD is $4\,\text{m}$.

III. COMMUNICATION SYSTEM MODEL
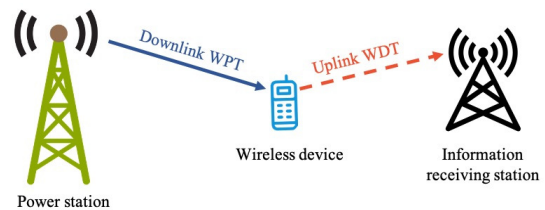
A. Network Model

Fig. 3. System Model

We consider a multiple-antenna WPCN with downlink wireless power transfer (WPT) and uplink wireless data transmission (WDT) (Fig. 3). We assume energy beamforming in the downlink. That is, the PS utilizes its multiple antennas to focus energy beams toward the WD. Energy beamforming thus maximizes the harvested energy at the WD [15], [39], [46]. To enable this, the PS performs MRT energy beamforming by properly weighting the transmit signals at different PS antennas, since MRT is optimal for the single-user case [46]. The beamforming vector in this case is $\mathbf{w}^* = \frac{\mathbf{h}}{||\mathbf{h}||}$. On the other hand, IRS uses maximum ratio combiner (MRC) reception of uplink signals with a combining weight vector $\mathbf{u}^* = \frac{\mathbf{g}}{||\mathbf{g}||}$ [15] where $\mathbf{g}$ is the uplink channel between the WD and the IRS. Following [15], [47], we assume the availability of perfect channel state information (CSI) at the WD and IRS. For a duration of one transmission block T, τT duration is used for downlink WPT, where $\tau \in (0, 1)$. The WD harvests energy in τT and then transmits data in the uplink WDT for $(1 - \tau)T$ duration. Without loss of generality, we assume a normalized unit transmission block time (i.e., $T = 1$).

B. Channel Models

The small-scale mutipath fading part of the WPT channel is denoted as $\mathbf{h} \in \mathbb{C}^{N \times 1}$, which is distributed as $\mathbf{h} \sim \mathcal{CN}(0, I_N)$.

Similarly, the WDT channel, i.e., WD-IRS is denoted as $\mathbf{g} \in \mathbb{C}^{M \times 1}$, which is distributed as $\mathbf{g} \sim \mathcal{CN}(0, I_M)$. $\mathbf{h}$ and $\mathbf{g}$ are independent. Clearly, all the channel coefficients $h_k, g_k \ \forall k \in [1, N]$ are independent and identically distributed (iid) $\mathcal{CN}(0, 1)$ RVs. Consider $||\mathbf{h}||^2 = \sum_{i=1}^{N} |h_i|^2$ and $||\mathbf{g}||^2 = \sum_{j=1}^{M} |g_j|^2$. Thus, both $||\mathbf{h}||^2$ and $||\mathbf{g}||^2$ are scaled central Chi-square random variables distributed with $2N$ and $2M$ degrees of freedom. Thus, theis PDF's are special cases of the following PDF:

$$f(x) = \frac{1}{\Gamma(L)} x^{L-1} e^{-x}, \quad 0 \le x < \infty, \tag{10}$$

where $L = N$ or $L = M$. The moment generating function (MGF) for this PDF is given by

$$M(t) = \mathbb{E}[e^{-tX}] = \frac{1}{(1+t)^L}, \quad \Re(t) > -1. \tag{11}$$

Although this MGF is well known, we list it here because the essential role it plays in our performance analysis. The role arises due to the fact that the received signal power at the WD contains a factor $||\mathbf{g}||^2$, which is Gamma distributed. Thus, this MGF will help the overall averaging process, which can actually be done in two stages. The first stage can be the averaging over the distribution of $||\mathbf{g}||^2$, which requires the MGF in (11). Moreover, the MGF method can be used for extensive analysis of communication links [48], [49].

The PS-WD and WD-IRS distances are d_1 and d_2 respectively. The large-scale pathlosses of the WPT and WDT channels are $\Omega_k = d_k^{-s}$ $(k = 1, 2)$ [50] where s is the path loss factor and d_k is the distance between the transmitter and the receiver, usually measured in meters [21].

C. Signal-to-Noise Ratio

Let P be the amount of power harvested by the WD. According to the four different EH models (Section II), we have $P = P_h$ for NLEH, $P = P_a$ for AM, $P = P_l$ for LM, and $P = P_{rat}$ for RM. The input RF power of the EH circuit is given by $P_r = \bar{P}_t ||\mathbf{h}||^2$. The WD harvests energy for duration τ. Thus, the amount of energy harvested by the WD is $E_h = P\tau$. The WD transmits signals to the IRS for a duration of $(1 - \tau)$. Suppose that the WD uses a power amplifier with efficiency $0 < \eta < 1$. Thus, ηE_h is used for data transmission in the WD-IRS link, and the power amplifier consumes the rest [39]. Hence, during the data transfer phase, the transmit power of the WD is $P_{WD} = \frac{\eta E_h G_{\text{WD}}}{(1-\tau)}$. Consequently, the signal-to-noise ratio (SNR) at the IRS can be written as

$$\gamma = \frac{\tau \eta P \Omega_2 G_{\text{WD}} G_{\text{IRS}} ||\mathbf{g}||^2}{(1-\tau)\sigma^2} = cP||\mathbf{g}||^2, \tag{12}$$

where G_{IRS} is the antenna gain of IRS and $c = \frac{\tau \eta \Omega_2 G_{\text{WD}} G_{\text{IRS}}}{(1-\tau)\sigma^2}$.

In the next section, we analyze the average throughput of delay-limited and delay-tolerant modes [15]. These modes are determined based upon the length of codewords transmitted by the user. If each codeword is short, and thus the IRS decodes each one without waiting to process multiple codewords together, the resulting mode is the delay limited mode. Consequently, in this case, outage probability (OP), the probability that the transfer rate below a given threshold, is the

relevant measure of the system throughput. In contrast, in the delay-tolerant mode, the IRS may store multiple codewords and decode them in one shot. The throughput in this case is measured by the long-term statistical average of the wireless channel capacity, i.e., ergodic capacity (EC).

IV. PERFORMANCE ANALYSIS WITH THE EH MODELS

Herein, we derive the average throughput of the delay-limited and delay-tolerant transmission modes as well as the average BER of BPSK and BDPSK modulations. The four EH models are considered. We derive integral expressions and/or closed-form expressions for these performance metrics and suggest a efficient and simple numerical evaluation method based on the generalized Gauss-Laguerre quadrature (Appendix A.)

A. New Energy Harvesting Model

1) Delay-Limited Transmission Mode

In this mode, the IRS decodes each codeword, without waiting for more them. So in this case, short-term rise and fall of SNR mediates the success of each decoding operation. Therefore, the throughput of this mode is appropriately measured by the OP. It is the probability that the instantaneous throughput, $\log_2(1 + \gamma_A)$, falls below a fixed rate R bits/s/Hz. Since the WD only transmits during the time fraction $(1 - \tau)$ with a fixed transmit rate R, the average throughput in bits/s/Hz can be expressed as

$$R_{DL} = (1 - P_{out}) R^*, \tag{13}$$

where $R^* = (1 - \tau) R$ and P_{out} is the OP. In the following proposition, we derive the delay-limited throughput.

Proposition 1. *The average throughput of delay-limited mode of the WD-IRS link with the NLEH model (1) is given by*

$$R_{DL} = R^* \left[1 - \frac{\int_0^\infty \gamma\left(M, \frac{\gamma_{th}}{cq(\bar{P}_t x)}\right) x^{N-1} e^{-x} dx}{\Gamma(N)\Gamma(M)} \right], \tag{14}$$

where $\gamma_{th} = 2^R - 1$ is a predetermined threshold. In (14), $\gamma(n, x)$ is the lower incomplete gamma function [44, Eq. (8.350)] and $\Gamma(a)$ is gamma function [44, Eq. (8.310.1)].

Proof. The proof is given in Appendix C. ∎

Remark 1. *The $q(x)$ function in (14) is the nonlinear EH model given in (1). Since $q(x)$ contains an error function, and if we submit $q(x)$ into (14), the integral function is too complicated, so the closed-form expression does not exit. However, (14) can be approximated by generalized Gauss-Laguerre quadrature given in Appendix A. The impact of parameters is not clear in (14), but it can be observed from Section VII.*

2) Delay-Tolerant Transmission Mode

When this mode is used, the codeword length is large compared to the block time. Thus, a large delay is tolerable for decoding the stored signals together. Thus, the average throughput of this mode is the product of ergodic capacity and the effective data transfer time, which can be shown in bits/s/Hz as

$$R_{DT} = (1 - \tau) C_e, \tag{15}$$

where C_e is the ergodic capacity. In the following proposition, we derive the delay-tolerant throughput.

Proposition 2. *The delay-tolerant throughput of the WDT link with the nonlinear EH model* (1) *is given by*

$$R_{DT} = \frac{(1 - \tau)}{\Gamma(N)\Gamma(M)} \int_0^\infty I_{M-1}\left(\frac{1}{cq(\bar{P}_t x)}\right) \frac{x^{N-1}e^{-x}}{(cq(\bar{P}_t x))^M} dx, \tag{16}$$

where $I_n(a)$ is the function given in Lemma 1 in Appendix B.

Proof. See the Appendix D. ∎

Remark 2. *The* (16) *can be evaluated by generalized Gauss-Laguerre quadrature via mathematical software, such as MAT-LAB. According to* (71)*, the number of summation terms n can be obtained by the following strategy. We write $W_i = \sum_{i=1}^n w_i f(x_i)$, $W_1 = w_1 f(x_1)$, and $W_i = W_{i-1} + w_i f(x_i)$. When $\frac{w_i f(x_i)}{W_i} \leq 0.01$, the series computation stops, and choose $n = i$.*

3) Average BER of BPSK

BPSK is a simple digital modulation that uses two phases, say, 0 and π to represent binary 0 and 1. Consequently, it can tolerate highest noise level or distortion than other higher-order modulations. Thus, BPSK is robust against thermal noise and other forms of noise as well as widely used in the standard IEEE 802.15.4 which is used by ZigBee [51]. In the following, we derive its BER as a simple integral.

Proposition 3. *The BER expression of the WD-IRS link with the nonlinear EH model* (1) *and BPSK modulation is given by*

$$\bar{P}_{BER} = \frac{1}{\Gamma(N)} \int_0^\infty x^{N-1} e^{-x} \left[\frac{1}{2}\left(1 - \sqrt{\frac{cq(\bar{P}_t x)}{1 + cq(\bar{P}_t x)}}\right)\right]^M$$

$$\cdot \sum_{k=0}^{M-1} \binom{M-1+k}{k} \left[\frac{1}{2}\left(1 + \sqrt{\frac{cq(\bar{P}_t x)}{1 + cq(\bar{P}_t x)}}\right)\right]^k dx. \tag{17}$$

Proof. See Appendix E. ∎

Remark 3. *Computationally, the BER expression* (17) *can be easily evaluated by the generalized Gauss-Laguerre quadrature rule given in Appendix A. It is observed that the specific relationship between parameters and the BER are not clearly visible. However, the relationship can be obtained through the numerical and simulation figures in Section VII.*

4) Average BER of BDPSK

In BDPSK modulation, the phase of the modulated signal is shifted relative to the previous carrier's phase. BDPSK is used by wireless LAN (local area network) standard, IEEE 802.11b-1999 as the basic rate of $1\,\mathrm{Mbit/s}$ [52].

Proposition 4. *The BER expression of the WDT link with the nonlinear EH model* (1) *and BDPSK modulation is given by*

$$\bar{P}_{BER} = \frac{1}{2\Gamma(N)} \int_0^\infty \frac{x^{N-1}e^{-x}}{\left[1 + cq(\bar{P}_t x)\right]^M} dx. \tag{18}$$

Proof. The proof is given in Appendix F. ∎

Remark 4. *The expressions of BPSK and BDPSK above are complicated and cannot be derived closed form. But we can easily evaluate them via the generalized Gauss–Laguerre quadrature described in Appendix A.*

B. Asymptotic Model

In order to compare with the NLEH, we analyze the same performance metrics in the previous subsection. The function $q_{as}(\cdot)$ for the AM case is given in (4).

1) Delay-Limited Transmission Mode

According to Proposition 1, the delay-limited throughput of the WD-IRS link with the nonlinear EH model (4) can be given by

$$R_{DL} = R^* \left[1 - \frac{\int_0^\infty \gamma\left(M, \frac{\gamma_{\text{th}}}{cq_{as}(\bar{P}_t x)}\right) x^{N-1}e^{-x}dx}{\Gamma(N)\Gamma(M)}\right]. \tag{19}$$

The relationships of the throughput and parameters like N and M are not directly visible, but it can be observed in the Section VII-A.

2) Delay-Tolerant Transmission Mode

Using Proposition 2, the delay-tolerant throughput of the WDT link with the nonlinear EH model (4) is derived as

$$R_{DT} = (1 - \tau) \mathbb{E}\left[\log_2\left(1 + cP_a \|\mathbf{g}\|^2\right)\right]$$

$$\overset{(a)}{=} \frac{(1 - \tau)}{\Gamma(N)\Gamma(M)} \int_0^\infty I_{M-1}\left(\frac{1}{cq_{as}(\bar{P}_t x)}\right) \frac{x^{N-1}e^{-x}}{(cq_{as}(\bar{P}_t x))^M} dx. \tag{20}$$

The $I_n(a)$ is a function of integral and it can be calculated as the finite summation in Lemma 1. Similar to Proposition 2, the integral can be evaluated by generalized Gauss-Laguerre quadrature.

3) Average BER of BPSK

The BER expression of the WD-IRS link with the nonlinear EH model (4) and BPSK modulation can be given as

$$\bar{P}_{BER} = \frac{1}{\Gamma(N)} \int_0^\infty x^{N-1} e^{-x} \left[\frac{1}{2}\left(1 - \sqrt{\frac{cq_{as}(\bar{P}_t x)}{1 + cq_{as}(\bar{P}_t x)}}\right)\right]^M$$

$$\cdot \sum_{k=0}^{M-1} \binom{M-1+k}{k} \left[\frac{1}{2}\left(1 + \sqrt{\frac{cq_{as}(\bar{P}_t x)}{1 + cq_{as}(\bar{P}_t x)}}\right)\right]^k dx. \tag{21}$$

This equation (21) can be obtained from Proposition 3 by replacing $q(\cdot)$ with $q_{as}(\cdot)$.

4) Average BER of BDPSK

The BER expression for the WDT link with the nonlinear EH model (4) and BDPSK modulation can be given as

$$\bar{P}_{BER} = \frac{1}{2\Gamma(N)} \int_0^\infty \frac{x^{N-1}e^{-x}}{\left[1 + cq_{as}\left(\bar{P}_t x\right)\right]^M} dx. \qquad (22)$$

This equation (22) is derived similar to Proposition 4. Thus, the proof is omitted. In the next subsection, we will derive the performance of the most widely used linear EH model.

C. Linear EH Model

Since this is the default one used for a variety of networks, several results are already available. We list them here for completeness.

1) Delay-Limited Transmission Mode

According to Proposition 1, the average throughput linear EH model (6) is derived as follows.

$$R_{DL} \overset{(a)}{=} R^* \left[1 - \frac{\int_0^\infty \gamma\left(M, \frac{\gamma_{\text{th}}}{c\mu\bar{P}_t x}\right) x^{N-1}e^{-x}dx}{\Gamma(N)\Gamma(M)} \right]$$

$$\overset{(b)}{=} R^* \left[1 - \int_0^\infty \frac{\left(1 - e^{-\frac{\gamma_{\text{th}}}{c\mu\bar{P}_t x}} \sum_{m=0}^{M-1} \left(\frac{\gamma_{\text{th}}}{c\mu\bar{P}_t x}\right)^m \frac{1}{m!}\right) x^{N-1}e^{-x}dx}{\Gamma(N)} \right]$$

$$\overset{(c)}{=} \frac{2R^*}{\Gamma(N)} \sum_{m=0}^{M-1} \left(\frac{\gamma_{\text{th}}}{c\mu\bar{P}_t}\right)^{\frac{N+m}{2}} \frac{1}{m!} K_{N-m}\left(2\sqrt{\frac{\gamma_{\text{th}}}{c\mu\bar{P}_t}}\right), \qquad (23)$$

where (a) is from Proposition 1; (b) is because of [44, Eq. (8.352.6)]; (c) is obtained from [44, Eq. (3.471)]. $K_\nu(\cdot)$ is the ν-th order modified Bessel function of the second kind [44, Eq. (8.432)]. The special case $N = M$ has been studied in [15, Eq. (5)]. The average throughput R_{DL} depends on τ, N, M, γ_{th}, P_t and μ. It does not offer explicit relationships of the above parameters. However, we can find the impact of parameters in Section VII.

2) Delay-Tolerant Transmission Mode

The average throughput of delay-tolerant mode for the linear EH model (6) can be derived as

$$R_{DT} = \frac{\frac{(1-\tau)}{c\mu\bar{P}_t} G_{2,4}^{4,1}\left(\frac{1}{c\mu\bar{P}_t} \middle| \begin{matrix} -1, 0 \\ -1, -1, M-1, N-1 \end{matrix}\right)}{\Gamma(N)\Gamma(M)\ln 2}, \qquad (24)$$

where $G_{pq}^{mn}\left(z \middle| \begin{matrix} a_1 \cdots a_p \\ b_1 \cdots b_q \end{matrix}\right)$ denotes the Meijer G-function [44, Eq. (9.301)]. and The special case $M = N$ of (24) has been derived in [15, Eq. (12)]. That same derivation can be used to prove (24). Thus, the details are omitted here. The average throughput R_{DT} depends on parameters τ, N, M, P_t and μ. However, insights can be derived from numerical evalution of (23).

3) Average BER of BPSK

The BER expression of the WD-IRS link with the linear EH model (6) and BPSK modulation is given by

$$\bar{P}_{BER} = \frac{1}{\Gamma(N)} \int_0^\infty x^{N-1}e^{-x}\left[\frac{1}{2}\left(1 - \sqrt{\frac{c\mu\bar{P}_t x}{1 + c\mu\bar{P}_t x}}\right)\right]^M$$

$$\cdot \sum_{k=0}^{M-1} \binom{M-1+k}{k}\left[\frac{1}{2}\left(1 + \sqrt{\frac{c\mu\bar{P}_t x}{1 + c\mu\bar{P}_t x}}\right)\right]^k dx. \qquad (25)$$

This is result is similar to Proposition 3. Thus, the proof is omitted.

This integral (25) can be very efficiently and simply calculated by the generalized Gauss-Laguerre quadrature described in Appendix A.

4) Average BER of BDPSK

The BER expression of the WD-IRS link with the linear EH model (6) and BDPSK modulation is given by

$$\bar{P}_{BER} \overset{(a)}{=} \frac{1}{2\Gamma(N)} \int_0^\infty \frac{x^{N-1}e^{-x}}{\left[1 + c\mu\bar{P}_t x\right]^M} dx$$

$$\overset{(b)}{=} \frac{1}{2\left(c\mu\bar{P}_t\right)^N} \Psi\left(N, N-M+1; \frac{1}{c\mu\bar{P}_t}\right), \qquad (26)$$

where (a) is obtained from Proposition 4; Step (b) is obtained from [44, Eq. (9.211.4)] and $\Psi(a,b;z)$ is the confluent hypergeometric function in [44, Eq. (9.211.4)].

In the next subsection, we derive the performances for the rational EH model.

D. Rational EH Model

1) Delay-Limited Transmission Mode

Similar to Proposition 1, the delay-limited throughput of the WDT link with the rational EH model (8) can be given by

$$R_{DL} = R^* \left[1 - \frac{\int_0^\infty \gamma\left(M, \frac{\gamma_{\text{th}}}{cq_{rat}\left(\bar{P}_t x\right)}\right) x^{N-1}e^{-x}dx}{\Gamma(N)\Gamma(M)} \right]. \qquad (27)$$

Since (27) is not closed-form, the relationships between R_{DL} and the parameters, for example, γ_{th}, N, and M from (27) are not directly visible. However, (27) is extremely easy to compute. Thus, insights can be obtained – see Section VII.

2) Delay-Tolerant Transmission Mode

The throughput of the WD-IRS link in this case with nonlinear EH model (8) can be given as

$$R_{DT} = (1-\tau)\,\mathbb{E}\left[\log_2\left(1 + cP_{rat}||\mathbf{g}||^2\right)\right]$$

$$\overset{(a)}{=} \frac{(1-\tau)}{\Gamma(N)\Gamma(M)} \cdot \int_0^\infty I_{M-1}\left(\frac{1}{cq_{rat}\left(\bar{P}_t x\right)}\right) \frac{x^{N-1}e^{-x}}{\left(cq_{rat}\left(\bar{P}_t x\right)\right)^M} dx. \qquad (28)$$

By replacing $q(\cdot)$ in Proposition 2 to $q_{rat}(\cdot)$, we obtain (28). The integral in (28) can be readily calculated by using Lemma 1 and the Gaussian-Laguerre quadrature (Appendix A.)

3) Average BER of BPSK

The BER of the WD-IRS link and the nonlinear EH model (8) and BPSK modulation can be obtained by

$$\bar{P}_{BER} = \frac{1}{\Gamma(N)} \int_0^\infty x^{N-1} e^{-x} \left[\frac{1}{2}\left(1 - \sqrt{\frac{cq_{rat}(\bar{P}_t x)}{1 + cq_{rat}(\bar{P}_t x)}}\right)\right]^M$$
$$\cdot \sum_{k=0}^{M-1} \binom{M-1+k}{k} \left[\frac{1}{2}\left(1 + \sqrt{\frac{cq_{rat}(\bar{P}_t x)}{1 + cq_{rat}(\bar{P}_t x)}}\right)\right]^k dx. \tag{29}$$

By replacing $q(\cdot)$ in Proposition 3 with $q_{rat}(\cdot)$, we can obtain (29).

4) Average BER of BDPSK

Proposition 5. *The BER of the WD-IRS link with the rational EH model* (8) *and BDPSK modulation can be expressed as*

$$\bar{P}_{BER} = \frac{\sum_{k=0}^M \binom{M}{k}\left(\frac{M\bar{P}_t}{\beta}\right)^k \left(\frac{\beta}{A}\right)^{N+k} \Gamma(N+k)}{2\Gamma(N)} \tag{30}$$
$$\cdot \Psi\left(N+k, N-M+k+1; \frac{\beta}{A}\right).$$

Proof. By using Proposition 4, we write the BER as Step (a) in the following:

$$\bar{P}_{BER} \overset{(a)}{=} \frac{1}{2\Gamma(N)} \int_0^\infty \frac{x^{N-1}e^{-x}}{\left[1 + cq_{rat}(\bar{P}_t x)\right]^M} dx$$
$$\overset{(b)}{=} \frac{1}{\Gamma(N)} \int_0^\infty \frac{x^{N-1}e^{-x}}{\left(1 + c\frac{M\bar{P}_t x}{M\bar{P}_t x + \beta}\right)^M} dx$$
$$\overset{(c)}{=} \frac{1}{2\Gamma(N)} \int_0^\infty \frac{x^{N-1}e^{-x}\left(M\bar{P}_t x + \beta\right)^M}{\left[Ax + \beta\right]^M} dx \tag{31}$$
$$\overset{(d)}{=} \frac{\sum_{k=0}^M \binom{M}{k}\left(\frac{M\bar{P}_t}{\beta}\right)^k \left(\frac{\beta}{A}\right)^{N+k} \Gamma(N+k)}{\Gamma(N)}$$
$$\cdot \Psi\left(N+k, N-M+k+1; \frac{\beta}{A}\right),$$

where $A = (1+c)M\bar{P}_t$; Step (b) follows from the rational model in (8); Let $u = \frac{Ax}{\beta}$ in (c), and with the help of [44, Eq. (9.211.4)], (d) is obtained after some algebraic manipulations. ∎

Remark 5. *Although* (31) *gives exact value of the average BER of BPSK, it does not show the direct relationships between the parameters N, M, β, and P_t because it contains a confluent hypergeometric function. However, by considering the large antenna case* ($N \to \infty$), *we can obtain simpler but accurate performance expressions.*

E. Large Antenna Case

Wireless systems with an especially high number of antennas, e.g., tens or even hundreds of antennas, are called massive MIMO. Systems with as many as 96 to 128 antennas have been demonstrated. MIMO network can multiply the capacity of a wireless connection without requiring more spectrum. Thus, large capacity improvements are possible. More antennas translate into more possible signal paths, which improves and data rate and link reliability [53], [54].

In the following, we consider the PS to be massive MIMO, e.g., $N \to \infty$. In this case, we will see a channel hardening effect.

Let the WPT channel gain be $X = ||\mathbf{h}||^2$ and in this case, $X \overset{d}{\to} \mathcal{N}(N, N)$. Recall the received power at the WD is $P_r = \bar{P}_t||\mathbf{h}||^2$. Thus $P_r \overset{d}{\to} \mathcal{N}\left(\bar{P}_t N, \bar{P}_t^2 N\right)$. In the previous section, we dealt with the problem of computing average throughput and BER in the format $\mathbb{E}[Y]$, where Y is a function of P_r, i.e. $Y = g(P_r)$. But evaluating $\mathbb{E}[Y]$ is not direct. To avoid this issue, we can expand Y around the mean of P_r, which is $\theta = \bar{P}_t N$. The quantity Y is expanded as

$$Y = g(\theta) + g'(\theta)(P_r - \theta) + \frac{1}{2}g''(\theta)(P_r - \theta)^2 + \cdots \tag{32}$$

By taking the expected value of both sides, we find

$$\mathbb{E}[Y] = g(\theta) + \frac{1}{2}g''(\theta)\mathbb{E}\left[(X - \theta)^2\right] + \cdots \tag{33}$$

The right side can be approximated as

$$\mathbb{E}[Y] \approx g(\theta) + E, \tag{34}$$

where the error term is given by

$$E = \frac{1}{2}g''(\theta)\bar{P}_t^2 N. \tag{35}$$

In general, it is difficult to estimate the magnitude of this error term. But in order to get at least some sense of this error term, we can evaluate it for the linear model in (26). In this case, we find $g(x) = \frac{1}{(1+tx)^M}$ where $t = c\mu\bar{P}_t$. By evaluating, this term for (35), we find that

$$E \approx \frac{M(M+1)}{t^M \bar{P}_t^M N^{M+1}} = O\left(\frac{1}{N^{M+1}}\right). \tag{36}$$

Thus, this error term vanishes rapidly when the number of PS antennas is large enough. Therefore, we expect (34) to be highly accurate in this case.

The asymptotic performance for large antenna case with the new EH model (1) can be derived by following the approximated results obtained in (34) as following propositions:

Proposition 6. *When the number of PS antennas increases without bound, i.e. $N \to \infty$, the asymptotic average throughput of delay-limited mode for the WD-IRS link with the NLEH (1) is given by*

$$R_{DL} = R^* \left[1 - \frac{1}{\Gamma(M)}\gamma\left(M, \frac{\gamma_{th}}{cq(\bar{P}_t N)}\right)\right]. \tag{37}$$

Compared to the exact result in (14), *the asymptotic result* (37) *is closed-form and simpler.*

Proposition 7. *When the PS antenna increases, $N \to \infty$, the asymptotic average throughput of delay-tolerant mode for the WD-IRS link with the NLEH (1) is given by*

$$R_{DT} = \frac{(1-\tau)}{\Gamma(M)\left(cq(\bar{P}_t N)\right)^M} I_{M-1}\left(\frac{1}{cq(\bar{P}_t N)}\right). \tag{38}$$

Proposition 8. *When the energy harvesting at the WD is modeled according to the NLEH model (1), the asymptotic*

average BER of BPSK over WD-IRS link for large N is given by

$$\bar{P}_{BER} = \left[\frac{1}{2} \left(1 - \sqrt{\frac{cq\left(\bar{P}_t N\right)}{1 + cq\left(\bar{P}_t N\right)}} \right) \right]^M$$
$$\cdot \sum_{k=0}^{M-1} \binom{M-1+k}{k} \left[\frac{1}{2} \left(1 + \sqrt{\frac{cq\left(\bar{P}_t N\right)}{1 + cq\left(\bar{P}_t N\right)}} \right) \right]^k. \tag{39}$$

In the large antenna case, we can simply (39) as

$$\bar{P}_{BER} \approx \left[\frac{1}{2} \left(1 - \sqrt{\frac{cP_{\max}}{1 + cP_{\max}}} \right) \right]^M$$
$$\cdot \sum_{k=0}^{M-1} \binom{M-1+k}{k} \left[\frac{1}{2} \left(1 + \sqrt{\frac{cP_{\max}}{1 + cP_{\max}}} \right) \right]^k \tag{40}$$

where $N \to \infty$.

Proposition 9. *When the WD utilizes NLEH (1) model to harvest energy, the asymptotic average BER of BDPSK over WD-IRS link for large N is obtained by using (18) as*

$$\bar{P}_{BER} = \frac{1}{2\left[1 + cq\left(\bar{P}_t N\right)\right]^M}. \tag{41}$$

(41) can be further simplified as

$$\bar{P}_{BER} = \frac{1}{2\sum_{k=0}^{M} \left(cP_{\max}\right)^k}. \tag{42}$$

The asymptotic expressions for the AM, LM, and RM models are easily derived similarly. We omit the details for brevity.

F. Impact of Transmit Power Control

In massive MIMO systems, power scaling laws describe how fast the transmission power can decrease with the increasing of the number of antennas while maintaining certain performance levels [55]. For example, [56] investigates massive MIMO relay networks with imperfect channel state information, co-channel interference. Overall, energy savings are possible. The following proposition describes the achievable throughput of our system when transmit power control is implemented.

Proposition 10. *When the number of PS antennas increases without a bound ($N \to \infty$), for transmit power control $P_t = \frac{P_0}{N}$, the average throughput of the delay-tolerant mode for the NLEH model is given as*

$$R_{DT} = \frac{(1-\tau)}{\Gamma(M)(cz)^M} I_{M-1}\left(\frac{1}{cz}\right), \tag{43}$$

where $z = P_{\max}\left[\frac{\mathrm{erf}(a(\bar{P}_0+b))-\mathrm{erf}(ab)}{1-\mathrm{erf}(ab)}\right]$ *and* $\bar{P}_0 = P_0\Omega_1 G_{PS} G_{WD}$.

Proof. Recall that $\mathbf{h} \sim \mathcal{CN}(0, I_N)$. When the number of PS antennas increases without a bound, the law of large numbers

suggests that $\frac{\mathbf{h}^H \mathbf{h}}{N} \xrightarrow{a.s.} 1$, where $\xrightarrow{a.s.}$ denotes almost sure convergence.

Recall $\gamma = \frac{\tau \eta P \Omega_2 G_{\mathrm{WD}} G_{\mathrm{IRS}} ||\mathbf{g}||^2}{(1-\tau)\sigma^2}$. For the NLEH model, we have $P = P_{\max}\left[\frac{\mathrm{erf}(a(\bar{P}_t||\mathbf{h}||^2+b))-\mathrm{erf}(ab)}{1-\mathrm{erf}(ab)}\right]$ and SNR can be written as $\gamma = cP_{\max}\left[\frac{\mathrm{erf}(a(\bar{P}_t||\mathbf{h}||^2+b))-\mathrm{erf}(ab)}{1-\mathrm{erf}(ab)}\right] ||\mathbf{g}||^2$. Assume $P_t = \frac{P_0}{N}$, where P_0 is a fixed value and $\bar{P}_t = \frac{\bar{P}_0}{N}$. When the number of PS antennas increases ($N \to \infty$), the SNR is given as $\lim_{N\to\infty} \gamma = cP_{\max}\left[\frac{\mathrm{erf}(a(\bar{P}_0+b))-\mathrm{erf}(ab)}{1-\mathrm{erf}(ab)}\right]||\mathbf{g}||^2 = cz||\mathbf{g}||^2$. Therefor, the throughput of the delay-tolerant mode is

$$\begin{aligned} R_{DT} &= \mathbb{E}\left[\log_2\left(1+\gamma\right)\right] \\ &= \mathbb{E}\left[\log_2\left(1+cz||\mathbf{g}||^2\right)\right] \\ &= \frac{(1-\tau)}{\Gamma(M)(cz)^M} I_{M-1}\left(\frac{1}{cz}\right). \end{aligned} \tag{44}$$

$\blacksquare$

Remark 6. *Note that (43) is a constant limit independent of the number of antennas. It shows that when the PS antennas N grows without a bound, the transmit power can be scaled down proportionally to $\frac{1}{N}$ to maintain the same capacity.*

V. RESOURCE ALLOCATION WITH NEW MODELS

In this section, we generalize the WPCN in Fig. 3 to a multi-user scenario with $K > 1$ single-antenna WDs. We aim to maximize the lowest demand on data rate, i.e., fairness, by optimizing energy beamformer $\mathbf{w} \in \mathcal{C}^{N \times 1}$ and time allocation τ. The multi-antenna PS transfers power to the WDs with a common energy beamforming vector $\mathbf{w}$ in the WPT phase subject to $||\mathbf{w}||_2^2 \le P_t$ [57]. While in the uplink, all the WDs transmit information to the IRS simultaneously via SDMA in the WDT phase, which thus has higher spectrum efficiency than orthogonal user transmissions in TDMA [10]. We will jointly optimize the energy beamformer $\mathbf{w}$ and time allocation τ to maximize the minimum rate of the uplink WDT with the four EH models: NLEH, AM, LM, and RM.

The PS transfers the power with a common energy beamforming vector $\mathbf{w}$ in the WPT phase subject to $||\mathbf{w}||_2^2 \le P_t$. The harvested energy at kth WD, is then given as

$$E_k = \tau q(\bar{\Omega}_{1,k}|\mathbf{h}_k^H \mathbf{w}|^2) \tag{45}$$

where $\bar{\Omega}_{1,k} = \Omega_{1,k} G_{\mathrm{PS}} G_{\mathrm{WD}}$ where $\Omega_{1,k}$ is the large-scale pathloss between PS and the kth WD in the WPT phase and $q(P_r)$ is given as (1), (4), (6) and (8) for NLEH, AM, LM, and RM, respectively.

In the WDT phase, all the WDs transmit their information simultaneously to the IRS by consuming a fraction of the harvested energy ($\eta E_k, \forall k$). The transmit power of the kth WD is given as

$$p_k = \frac{\eta G_{\mathrm{WD}} E_k}{1-\tau} = \frac{\tau \eta G_{\mathrm{WD}}}{1-\tau} q(\bar{\Omega}_{1,k}|\mathbf{h}_k^H \mathbf{w}|^2). \tag{46}$$

The signal received at the IRS in the WDT phase ($\mathbf{y} \in \mathcal{C}^{M \times 1}$) can be expressed as

$$\mathbf{y} = \mathbf{G}\mathbf{x} + \mathbf{n}, \tag{47}$$

where $\mathbf{G} = [\mathbf{g}_1, \mathbf{g}_2, \ldots, \mathbf{g}_K]$ is the channel matrix, $\mathbf{x} = [x_1, x_2, \ldots, x_K]^T \sim \mathcal{CN}(\mathbf{0}, \mathbf{P})$ is the symbol vector with covariance matrix $\mathbf{P} = \text{diag}(p_1, p_2, \ldots, p_K)$, and $\mathbf{n} \sim \mathcal{CN}(\mathbf{0}, \sigma^2 \mathbf{I})$ is the noise vector at the IRS. The IRS applies zero-forcing (ZF) beamforming to decode the received data, $\mathbf{x}$, i.e., $\mathbf{U}^H = (\mathbf{G}^H \mathbf{G})^{-1} \mathbf{G}^H$. Hence, the instantaneous SNR in detecting x_k is given as

$$\gamma_k = \frac{\tau}{1-\tau} \bar{\gamma}_k(\mathbf{w}), \tag{48}$$

where, $\bar{\gamma}_k(\mathbf{w}) = \alpha_k q(\bar{\Omega}_{1,k}|\mathbf{h}_k^H \mathbf{w}|^2)$, in which $\alpha_k = \eta \Omega_{2,k} G_{\text{WD}} G_{\text{IRS}} / [\sigma^2 [(\mathbf{G}^H \mathbf{G})^{-1}]_{k,k}]$, where $\Omega_{2,k}$ is the large-scale pathloss between the kth WD and the IRS in the WDT phase.

The achievable sum rate for the kth WD is then given as

$$R_k(\mathbf{w}, \tau) = (1-\tau)\log_2\left(1 + \frac{\tau}{1-\tau} \bar{\gamma}_k(\mathbf{w})\right), \quad \forall k. \tag{49}$$

In the following, we will optimize the energy beamforming $\mathbf{w}$ and time allocation τ to maximize the minimum rate of the WDs, as follows,

$$\max_{\mathbf{w} \in \mathbb{C}^N, \tau \in \mathbb{R}} \left\{\min_{1 \le k \le K} R_k(\mathbf{w}, \tau)\right\}$$
$$\text{s.t. } \|\mathbf{w}\|_2^2 \le P_t, \quad 0 < \tau < 1. \tag{50}$$

The optimization problem in (50) can be solved in two steps. First, for fixed τ, we optimize the beamforming vector $\mathbf{w}$, as

$$\max_{\mathbf{w} \in \mathbb{C}^N} \left\{\min_{1 \le k \le K} R_k(\mathbf{w}, \tau)\right\} \quad \text{s.t. } \|\mathbf{w}\|_2^2 \le P_t. \tag{51}$$

Then, we optimize the value of τ, as

$$\max_\tau \min_{1 \le k \le K} R_k(\mathbf{w}^\dagger(\tau), \tau) \quad \text{s.t. } 0 < \tau < 1. \tag{52}$$

where $\mathbf{w}^\dagger(\tau)$ is the conditionally optimal solution to (51).

Due to the non-decreasing property of $\log_2(1+x)$, problem (51) can be formulated as

$$\max_{\mathbf{w} \in \mathbb{C}^N} \left\{\min_{1 \le k \le K} \bar{\gamma}_k(\mathbf{w})\right\} \quad \text{s.t. } \|\mathbf{w}\|_2^2 \le P_t, \tag{53}$$

which does not depend on τ. Hence, the optimal solution to (53) can be written as $\mathbf{w}^\dagger = \mathbf{w}^\dagger(\tau)$. Problem (52) can then be formulated as

$$\max_\tau (1-\tau) \log_2 \left(1 + \frac{\tau}{1-\tau} \min_{1 \le k \le K} \bar{\gamma}_k(\mathbf{w}^\dagger)\right)$$
$$\text{s.t. } 0 < \tau < 1. \tag{54}$$

The optimization problem in (54) is a convex optimization problem and can be solved numerically with computationally efficient off-the-shelf convex programs solvers. However, the beamforming optimization problem in (53) is challenging and can not be directly solved with convex optimization solvers. In the following, we will thus focus on this energy beamforming problem.

VI. ENERGY BEAMFORMING OPTIMIZATION

The optimal energy beamformer $\mathbf{w}$ should lie in the column space of the channel matrix $\mathbf{H}$ which is given as $\mathbf{H} = [\mathbf{h}_1, \mathbf{h}_2, \ldots, \mathbf{h}_K]$, to make the input power ($P_r = \bar{\Omega}_{1,k}|\mathbf{h}_k^H \mathbf{w}|^2$) as large as possible under the constraint $\|\mathbf{w}\|_2^2 \le P_t$ [40], [57]. Therefore, the energy beamformer can be written as $\mathbf{w} = \mathbf{F}\mathbf{v}$, where $\mathbf{v} \in \mathbb{C}^{r \times 1}$ is a weight vector and matrix $\mathbf{F} \in \mathbb{C}^{N \times r}$ forms an orthonormal basis for the column space of $\mathbf{H}$ with $r = \text{rank}(\mathbf{H})(\le \min(N, K))$ and $\mathbf{F}^H \mathbf{F} = \mathbf{I}$. Hence

$$|\mathbf{h}_k^H \mathbf{w}|^2 = |\tilde{\mathbf{h}}_k^H \mathbf{v}|^2, \tag{55}$$

where $\tilde{\mathbf{h}}_k = \mathbf{F}^H \mathbf{h}_k$. Therefore, the optimization problem in (53) can be written as

$$\max_{\mathbf{v} \in \mathbb{C}^r} \left\{\min_{1 \le k \le K} \alpha_k q(\bar{\Omega}_{1,k}|\tilde{\mathbf{h}}_k^H \mathbf{v}|^2)\right\} \quad \text{s.t. } \|\mathbf{v}\|_2^2 \le P_t. \tag{56}$$

By introducing a non-negative variable t, the max-min optimization problem in (56) can be written as

$$\max_{\mathbf{v} \in \mathbb{C}^r, t \in \mathbb{R}_+} t$$
$$\text{s.t. } \alpha_k q\left(\bar{\Omega}_{1,k}|\tilde{\mathbf{h}}_k^H \mathbf{v}|^2\right) \ge t, \quad \forall k,$$
$$\|\mathbf{v}\|_2^2 \le P_t, \tag{57}$$

which is not convex because the first constraint from the intersections of the nonconvex sets and $q(P_r)$ is not convex for nonlinear energy harvesting model. Hence, in the following, for each EH model, we will find a locally optimum solution for the value of $\mathbf{v}$, i.e., $\mathbf{w}$, through successive convex approximation (SCA) algorithm [58] by solving a set of sequential approximate convex subproblems. we must note that although we are unable to comment on the quality of the locally optimum solution, it has been shown that the output of the SCA algorithm is close to the globally optimal solution [59].

A. New Energy Harvesting Model

With NLEH model, by substituting (1) in (57), the optimization problem is given as

$$\max_{\mathbf{v} \in \mathbb{C}^r, t \in \mathbb{R}_+} t$$
$$\text{s.t. } \alpha_k P_{\max} \left[\frac{\text{erf}\left(a\bar{\Omega}_{1,k}|\tilde{\mathbf{h}}_k^H \mathbf{v}|^2 + ab\right) - \text{erf}(ab)}{1 - \text{erf}(ab)}\right] \ge t, \quad \forall k,$$
$$\|\mathbf{v}\|_2^2 \le P_t, \tag{58}$$

We may use $t = e^{-\tilde{t}}$ for $\tilde{t} \in \mathbb{R}$, then

$$\min_{\mathbf{v} \in \mathbb{C}^r, \tilde{t} \in \mathbb{R}} \tilde{t}$$
$$\text{s.t. } e^{-\tilde{t}} - \alpha_k P_{\max} \left[\frac{\text{erf}\left(a\bar{\Omega}_{1,k}|\tilde{\mathbf{h}}_k^H \mathbf{v}|^2 + ab\right) - \text{erf}(ab)}{1 - \text{erf}(ab)}\right] \le 0, \quad \forall k,$$
$$\|\mathbf{v}\|_2^2 \le P_t, \tag{59}$$

The nonlinear optimization problem in (59) is non-convex because the first constraint is not convex. Consequently, we solve it through SCA algorithm [58]. The essence of SCA is to solve through solving a sequence of approximate convex subproblems, which are obtained by approximating the non-convex constraints. In the SCA, the nonconvex constraint are typically convexified based on the first-order Taylor series truncation. To do so, $\rho_k(\mathbf{v}) = |\tilde{\mathbf{h}}_k^H \mathbf{v}|^2$ is replaced with its linear approximation from the first-order Taylor series around any feasible vector $\hat{\mathbf{v}}$, as [40], [59]

$$\hat{\rho}_k(\mathbf{v}, \hat{\mathbf{v}}) = |\tilde{\mathbf{h}}_k^H \hat{\mathbf{v}}|^2 + 2\Re\left\{\hat{\mathbf{v}}^H \tilde{\mathbf{h}}_k \tilde{\mathbf{h}}_k^H (\mathbf{v} - \hat{\mathbf{v}})\right\}, \quad (60)$$

where $\hat{\rho}_k(\mathbf{v}, \hat{\mathbf{v}}) \leq \rho_k(\mathbf{v})$ due to the convexity of $\rho_k(\mathbf{v})$.

The first constraint in (59) can be replaced with

$$\zeta_k(\tilde{t}, \hat{\rho}_k(\mathbf{v}, \hat{\mathbf{v}})) \leq 0, \quad \forall k, \quad (61)$$

where $\zeta_k(\tilde{t}, \rho) = e^{-\tilde{t}} - \alpha_k[\text{erf}(a\bar{\Omega}_{1,k}\rho + ab) - \text{erf}(ab)]$.

Due to the convexity of $\rho_k(\mathbf{v})$ and its first Taylor approximation, $\zeta_k(\tilde{t}, \rho_k(\mathbf{v})) \leq \zeta_k(\tilde{t}, \hat{\rho}_k(\mathbf{v}, \hat{\mathbf{v}}))$ for the nonincreasing function $\zeta_k(\tilde{t}, \rho)$ of ρ. Hence, equation (61) holds for any vector $\mathbf{v}$ satisfying the first constraint in (59) and the optimal solution of the approximate problem definitely belongs to the feasible set of the original optimization problem in (59).

The SCA algorithm iteratively solves the following problem:

$$\max_{\mathbf{v}_l \in \mathbb{C}^r, \tilde{t}_l \in \mathbb{R}} \tilde{t}_l$$
$$\text{s.t. } \zeta_k(\tilde{t}_l, \hat{\rho}_k(\mathbf{v}_l, \mathbf{v}_{l-1})) \leq 0, \quad \forall k,$$
$$\|\mathbf{v}_l\|_2^2 \leq P_t, \quad (62)$$

where $\mathbf{v}_{l-1}$ is the solution obtained in the previous iteration and $\mathbf{v}_0$ is selected randomly from the feasible set. Each convex subproblem in (62) can be efficiently solved using the convex optimization techniques such as the interior-point methods.

B. Asymptotic Model

In this case, by substituting (4) in (57), the optimization problem is given as

$$\max_{\mathbf{v} \in \mathbb{C}^r, t \in \mathbb{R}_+} t$$
$$\text{s.t. } \alpha_k P_{\max}\left(1 - e^{-\kappa\bar{\Omega}_{1,k}|\tilde{\mathbf{h}}_k^H \mathbf{v}|^2}\right) \geq t, \quad \forall k,$$
$$\|\mathbf{v}\|_2^2 \leq P_t. \quad (63)$$

The optimization problem in (63) is nonconvex because the first constraint is not convex. We may solve the optimization problem through the SCA algorithm and find an approximate solution by replacing the $|\tilde{\mathbf{h}}_k^H \mathbf{v}|^2$ with its first order Taylor expansion (its lower bound) given in (60). The convexity of $\rho_k(\mathbf{v})$ and the first-order Taylor approximation ensure that the optimal solution of the approximate problem belongs to the feasible set of the original optimization problem in (63). Hence, we can replace the first constraint in (63) with

$$\zeta_k(t, \hat{\rho}_k(\mathbf{v}, \hat{\mathbf{v}})) \leq 0, \forall k \quad (64)$$

where $\zeta_k(t, \rho) = \frac{1}{\alpha_k P_{\max}}t + e^{-\kappa\bar{\Omega}_{1,k}\rho} - 1$. Then we employ SCA algorithm to iteratively solve the problem

$$\max_{\mathbf{v}_l \in \mathbb{C}^r, t_l \in \mathbb{R}_+} t_l$$
$$\text{s.t. } \zeta_k(t_l, \hat{\rho}_k(\mathbf{v}_l, \mathbf{v}_{l-1})) \leq 0, \quad \forall k,$$
$$\|\mathbf{v}_l\|_2^2 \leq p_t, \quad (65)$$

where $\mathbf{v}_{l-1}$ is the solution which is obtained in the previous iteration and $\mathbf{v}_0$ is selected randomly from the feasible set. Each convex subproblem in (65) can be efficiently solved using the convex optimization techniques such as the interior-point methods.

C. Linear model

In this case, by substituting (6) in (57), the optimization problem is given as

$$\max_{\mathbf{v} \in \mathbb{C}^r, t \in \mathbb{R}_+} t$$
$$\text{s.t. } \alpha_k \bar{\Omega}_{1,k}\mu|\tilde{\mathbf{h}}_k^H \mathbf{v}|^2 \geq t, \quad \forall k,$$
$$\|\mathbf{v}\|_2^2 \leq P_t, \quad (66)$$

As this problem does not have a closed-form solution [60], we may use the SCA algorithm to find an approximate solution. Hence, using (60), the SCA algorithm iteratively solves the problem

$$\max_{\mathbf{v}_l \in \mathbb{C}^r, t_l \in \mathbb{R}_+} t_l$$
$$\text{s.t. } \zeta_k(t_l, \hat{\rho}_k(\mathbf{v}_l, \mathbf{v}_{l-1})) \leq 0, \quad \forall k,$$
$$\|\mathbf{v}_l\|_2^2 \leq P_t, \quad (67)$$

where $\zeta_k(t, \rho) = t - (\alpha_k \bar{\Omega}_{1,k}\mu)\rho$.

D. Rational model

With the RM model, the optimization problem is given as

$$\max_{\mathbf{v} \in \mathbb{C}^r}\left\{\min_{1 \leq k \leq K} \alpha_k P_{\max}\frac{|\tilde{\mathbf{h}}_k^H \mathbf{v}|^2}{|\tilde{\mathbf{h}}_k^H \mathbf{v}|^2 + \bar{\Omega}_{1,k}^{-1}\beta}\right\} \quad \text{s.t. } \|\mathbf{v}\|_2^2 \leq P_t. \quad (68)$$

In order to solve (68) and find the optimal value of $\mathbf{v}$, we employ the well-known Dinkelbach procedure, which has been introduced as an efficient method for solving quadratic fractional programming problems [61], [62]. The convergence properties of this algorithm are well established, and the rate of convergence is at least superlinear [62].

Using the Dinkelbach-type procedure, the fractional objective function can be replaced by a parametric quadratic function as follows [62]:

$$F(\lambda) = \max_{\mathbf{v} \in \mathbb{C}^r}\left\{\min_{1 \leq k \leq K}\left(\alpha_k P_{\max}|\tilde{\mathbf{h}}_k^H \mathbf{v}|^2 - \lambda\left(|\tilde{\mathbf{h}}_k^H \mathbf{v}|^2 + \bar{\Omega}_{1,k}^{-1}\beta\right)\right)\right\}$$
$$\text{s.t. } \|\mathbf{v}\|_2^2 \leq P_t. \quad (69)$$

where $\lambda \in \mathcal{R}$ is a constant. Then, an iterative algorithm is developed on λ to find a value λ^* such that $|F(\lambda^*)| < \epsilon$ (optimality tolerance).

Algorithm 1 summarizes the steps to find the optimal solution of (69).

Algorithm 1: Optimal beamformer with RM

1. Let $\mathbf{v}^0 \in$ feasible set, $\lambda_0 = \min\limits_{1 \le k \le K} \frac{\alpha_k P_{\max} |\tilde{\mathbf{h}}_k^H \mathbf{v}^0|^2}{|\tilde{\mathbf{h}}_k^H \mathbf{v}^0|^2 + \bar{\Omega}_{1,k}^{-1}\beta}$, and $i = 0$.

2. Determine an optimal solution $\mathbf{v}^i$ by solving (69) for $\lambda = \lambda_i$.

3. If $|F(\lambda_i)| < \epsilon$, $\mathbf{v}^i$ is the optimal solution and λ_i is the optimal value and STOP.

4. Let

$$\lambda_{i+1} = \min\limits_{1 \le k \le K} \frac{\alpha_k P_{\max} |\tilde{\mathbf{h}}_k^H \mathbf{v}^i|^2}{|\tilde{\mathbf{h}}_k^H \mathbf{v}^i|^2 + \bar{\Omega}_{1,k}^{-1}\beta}.$$

Replace i by $i+1$ and repeat step 2.

TABLE II
SIMULATION PARAMETERS

Parameter	Description	Value
T	Block duration	1
d_1	PS-WD distance	4 m
d_2	WD-IRS distance	10 m
s	Path loss exponent	2.8
σ^2	Noise variance	-60 dBm
a	Best fit [21]	0.0086
b	Best fit [21]	11.8689 μW
$P_{\max}$	Maximum harvested power	10.219 μW
G_{PS}	Antenna gain at PS	11 dBi
G_{WD}	Antenna gain at WD	3 dBi
G_{IRS}	Antenna gain at IRS	11 dBi

Note that in Algorithm 1, we have always $\lambda_i < \min_{1 \le k \le K}(P_{\max}\alpha_k)$. The optimization problem in (69) could be solved similar to LM through SCA, by substituting $|\tilde{\mathbf{h}}_k^H \mathbf{v}|^2$ with its first-order Taylor expansion (its lower bound) given in (60).

Remark 7. *In order to solve the convex subproblems of the iterative algorithms for NLEH, AM, LM and RM respectively given as (62), (65), (67) and (69) (similar to LM), we have applied interior-point methods. The SCA with NLEH requires a computational complexity estimate of at least $\mathcal{O}(r^3)$ to obtain the Newton steps of $\mathcal{O}(r)$ variables given by the linear equations for each iteration of interior-point method, while AM function requires a computational complexity estimate of $\mathcal{O}(r^3)$ to obtain the Newton steps of $\mathcal{O}(r)$ variables [40], [63]. Moreover, for LM and RM, in each iteration, we solve a SOCP with a per-iteration worst case complexity estimate of $\mathcal{O}(r^3)$.*

VII. NUMERICAL AND SIMULATION RESULTS

Herein, we provide extensive numerical results based on our analytical derivations and simulation results based upon Monte-Carlo simulations. The latter helps us to validate the former. Table II provides the key parameters. The NLEH model (1) parameters are obtained by standard curve fitting using the data set [21, Fig. (17.d)]. The parameters of the other three models are then computed based upon Section II. We assume $P_{se} = 0$ in Section VII, which results in $a = 0.0086$, $b = 11.8689$ and $P_{\max} = 10.219 \mu$W.
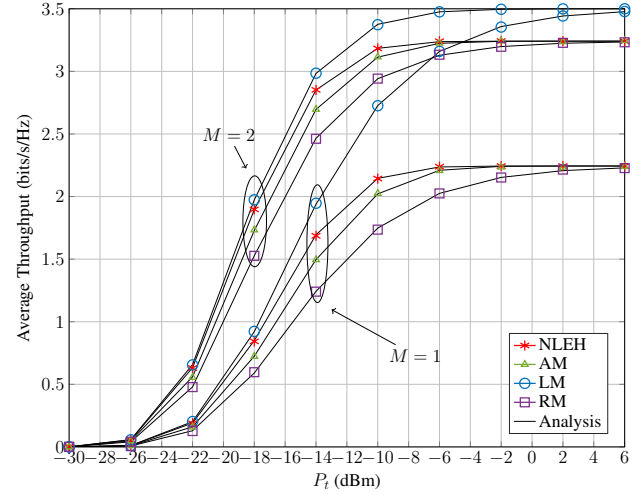

Fig. 4. Average throughput of delay-limited transmission mode versus P_t for $\tau = 0.3$, $R = 5$ bits/s/Hz, $N = 4$, and $\eta = 0.4$. The markers represent simulation points.

A. Throughput of the Delay-Limited Mode

Fig. 4 plots the average throughput of delay-limited mode versus the PS transmit power (P_t) for different numbers of IRS antennas (M). Fig. 4. yields several observations. First, the throughput for the four EH models increases first and then converges to a plateau as P_t increases. This coincides with the delay-limited throughput analytical results obtained in Section IV, for example, (14), (19), (23) and (27). Second, among these models, The LM model suggests the largest throughput, which indicates the overoptimistic nature of LM. Finally, one sees that increases M can improve the delay-limited throughput; for instance, with $P_t = -14$ dBm and NLEH model, average throughput increases from 1.6 bits/s/Hz for $M = 1$ to 2.7 bits/s/Hz for $M = 2$. The reason is that the IRS uses MRC to receive signals, more antennas can improve the performance.

Fig. 5 shows the effect of transmit rate (R) on the average throughput of delay-limited transmission mode for four different EH models. Obviously, the values of average throughput rise first and then drop to 0. According to (13) and (79), the average throughput of delay-limited mode is given as $R_{DL} = R(1-\tau)\left[1 - \Pr\left(\gamma < 2^R - 1\right)\right]$. From this equation, we can obtain that $R_{DL} \to 0$ when $R \to 0$ or $R \to \infty$, which matches the results shown in Fig. 5. Besides, the upper bound on the average throughput is $R(1-\tau)$. In order to achieve highest average throughput of delay-limited mode, we choose the values of R as $R = 5.5$ bits/s/Hz for LM and NLEH mode, $R = 5$ bits/s/Hz for AM and RM.

B. Throughput of the Delay-Tolerant Mode

Fig. 6 shows the average throughput of delay-tolerant mode versus the transmit power (P_t) at the PS for EH time fraction $\tau = 0.6$, number of PS antennas $N = 2$, number of IRS antennas $M = 2$, and power amplifier efficiency at WD $\eta = 0.8$ or $\eta = 0.4$. The throughput improves with increasing η since
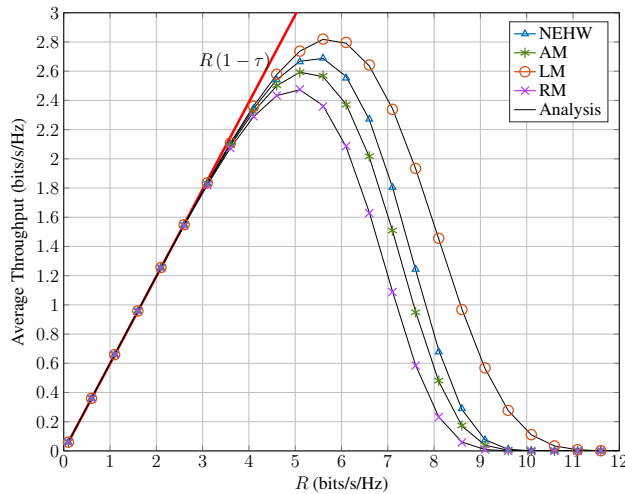
Fig. 5. Average throughput of delay-limited transmission mode versus R for $P_t = -10\,\text{dBm}$, $\tau = 0.4$ and $\eta = 0.4$, $N = 2$, and $M = 2$.

Fig. 7. Average throughput of delay-tolerant mode versus N for $P_t = -15\,\text{dBm}$, $\tau = 0.7$ and $\eta = 0.6$. The markers represent simulation points.
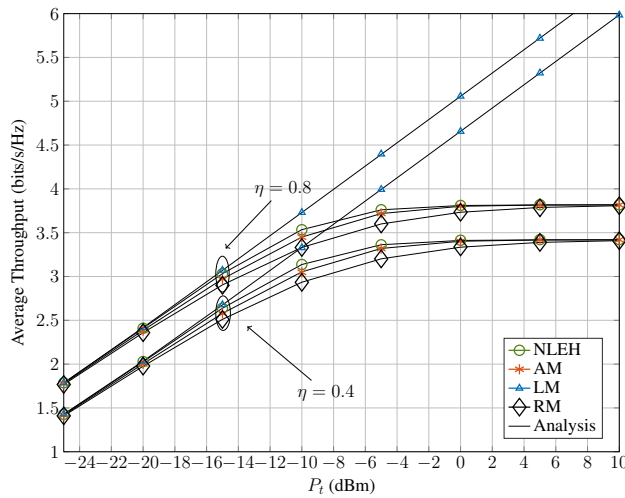

Fig. 6. Average throughput of the delay-tolerant mode versus P_t for $\tau = 0.6$, $N = 2$, and $M = 2$. The markers represent simulation points.

Fig. 8. Average throughput of delay-tolerant mode versus τ for $N = 2$, $M = 3$, and $\eta = 0.6$. The markers represent simulation points.

more harvested energy is used for information transmitted in the WD-IRS link. The average throughput is also improved by increasing the transmit power at the PS. However, the trends of the increment are different for the linear EH model and nonlinear EH models. Specifically, the throughput with nonlinear models tends to be saturated to maximum values ($3.8\,\text{bits/s/Hz}$ for $\eta = 0.8$ and $3.3\,\text{bits/s/Hz}$ for $\eta = 0.4$) when the transmit power of the PS is high enough. However, the average throughput of LM model grows monotonically as the PS transmit power increases. Clearly, this model fails to match the saturation property of practical EH circuits.

Fig. 7 plots the average throughput of delay-tolerant transmission mode versus the number of PS antennas (N) for transmit power $P_t = -15\,\text{dBm}$, energy harvest time fraction $\tau = 0.7$, and power amplifier efficiency at WD $\eta = 0.6$. The number of IRS antennas (M) is either 2 or 4. It is seen that
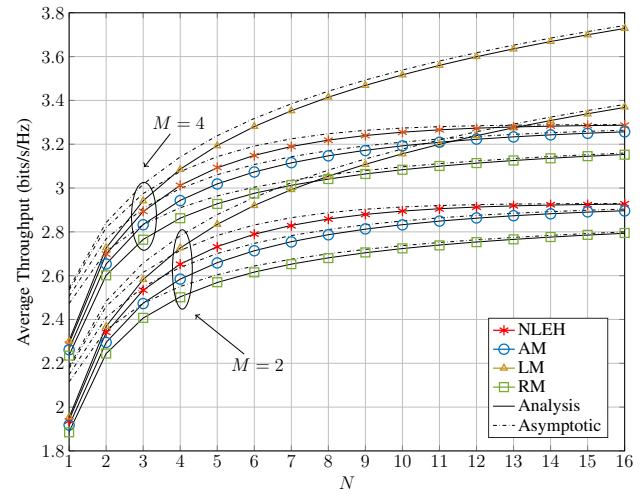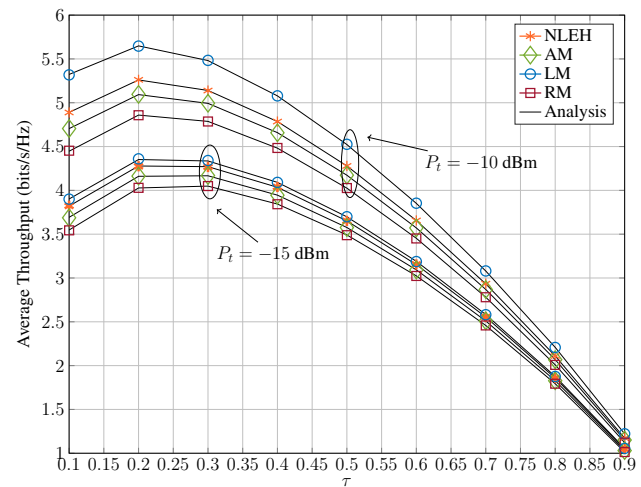
the value of average throughput for $M = 4$ is larger than that $M = 2$ which indicates adding more antennas at the IRS improves the throughput. We see that the asymptotic results (dashed lines) quickly approach the exact (solid lines) and simulation curves as the number of AP antennas increases. Besides, increasing the number of PS antennas boosts the average throughput of delay-tolerant mode when $N \leq 7$ and for $N > 7$, the saturation status is shown in nonlinear models whereas the curves of LM increasing without bound. Thus, LM is not appropriate for modeling the practical EH system. Especially when the transmit power is large. Fig. 8 plots the average throughput of delay-tolerant mode versus EH time fraction τ to demonstrate the impact of τ to this mode. It can be seen that a throughput-optimal EH time exists for four EH models. The optimal EH time for four EH models are around $\tau = 0.2$, which balances the downlink EH, and uplink
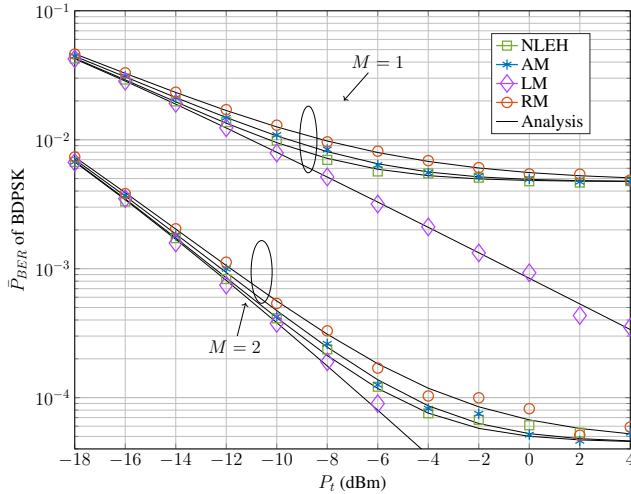
Fig. 9. $\bar{P}_{BER}$ versus P_t for $\tau = 0.4$, $N = 2$ and $\eta = 0.6$. The markers represent simulation points.

Fig. 10. $\bar{P}_{BER}$ versus N for $P_t = -18\,\text{dBm}$, $M = 2$, and $\eta = 0.4$. The markers represent simulation points.

information transfer, perfectly. Moreover, average throughput can be improved by increasing the transmit power at the PS.

C. BER performance

In Fig. 9, the average BER of BDPSK versus transmit power (P_t) at the PS is investigated. The BERs of nonlinear EH models, i.e., NLEH, AM and RM models, first decrease and then flatten as the transmit power of the PS increases. In contrast, the LM model suggests that the BER decreases arbitrarily as P_t increases. These coincide with the characteristics of four EH models shown in Fig. 1. Therefore, using the LM in WPCN system design may result in misleading and wrong conclusions. However, nonlinear EH models show more practical performances. Moreover, Fig. 9 also shows adding more antennas at the PS reduces BER of the system significantly.

Fig. 10 shows the BER of BDPSK versus the number of PS antennas (N) for transmit power $P_t = -18\,\text{dBm}$, power amplifier efficiency at WD $\eta = 0.4$, and number of IRS antenna $M = 2$. Fig. 11 plots the BER of BPSK versus N for $P_t = -20\,\text{dBm}$, $\tau = 0.5$, and $M = 2$. The red horizontal lines in both figures are asymptotic results derived from (42) and (40), respectively. It can be seen that red lines are lower bound for nonlinear EH models whereas LM does not have lower bound. Increasing the number of PS transmit antennas decreases the BER in both figures. Dashed lines are asymptotic results which gradually tend to the exact values (solid lines) as N increases in both figures. It is also observed that LM has smallest BER values of BDPSK and BPSK but this only works for small transmit power region. In Fig. 10, BER of BDPSK for $\tau = 0.5$ outperforms the one for $\tau = 0.3$ and in Fig. 11, we see that BER is improved by increasing η.

D. Resource Allocation

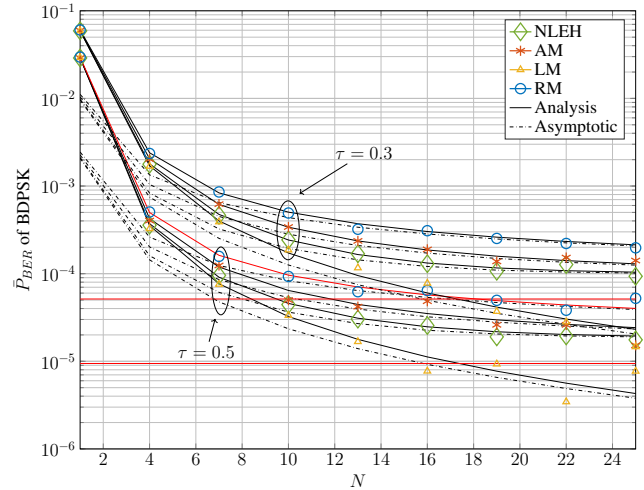Fig. 12 and Fig. 13 depict the max-min rate of the four EH models versus the number of antennas at the PS (N) for
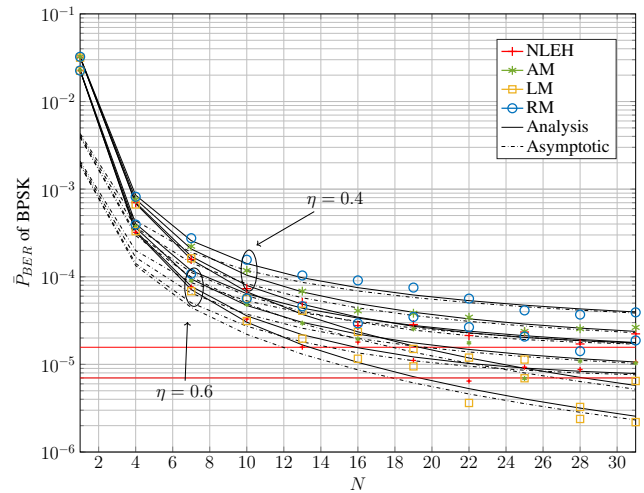

Fig. 11. $\bar{P}_{BER}$ versus N for $P_t = -20\,\text{dBm}$, $M = 2$, and $\tau = 0.5$. The markers represent simulation points.

transmit power $P_t = -15$ dBm, power amplifier efficiency at WD $\eta = 0.6$ and the number of IRS antennas $M = 7$. The number of WDs (K) are either 3 or 5. In order to investigate the performance improvement by designing energy beamforming in the WPT phase, we also consider the WPCN system powered by energy broadcasting without beamforming, i.e., the omni-directional beamforming [64]. The energy broadcasting is of low complexity and being widely used in commercial RF-energy-harvesting products [65]. For omni-directional beamforming, the PS broadcasts energy in all directions, i.e., the weight vector $\mathbf{w} = \sqrt{P_t/N}[1\ 1\ldots1]^T$.

Fig. 12 demonstrate the max-min rate for $K = 3$. As expected, compared to omni-directional beamformnig, optimal design of the energy beamformer significantly improves the performance of the WDs in terms of achievable rate. Considering the optimal performance, the achieved rate through
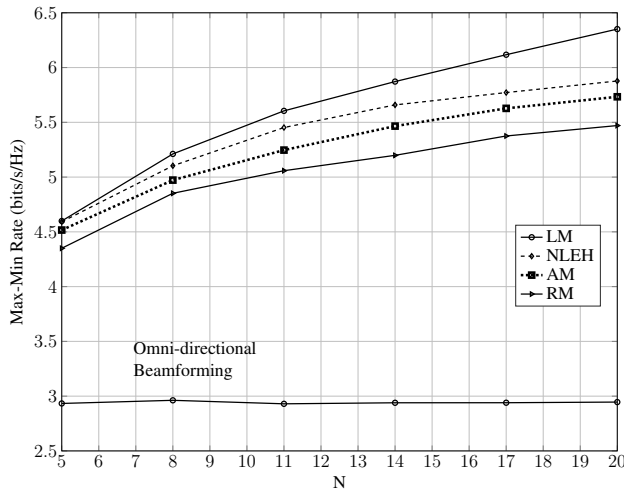
Fig. 12. Max-min rate versus N for $K = 3$, $M = 7$, $P_t = -15$ dBm and $\eta = 0.6$.
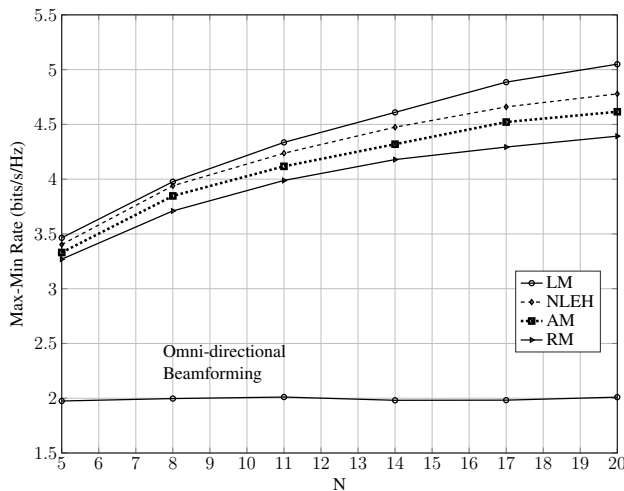

Fig. 13. Max-min rate versus N for $K = 5$, $M = 7$, $P_t = -15$ dBm and $\eta = 0.6$.

the NLEH is lower than that for the LM because $P_h < P_l$ (coincides with the comparison presented in Fig. 2). Moreover, RM achieves the lowest rate. In particular, to achieve a max-min rate at 5.5 bits/s/Hz, the NLEH, AM and RM respectively require about 11, 14 and 20 antennas at the PS, while the LM requires fewer PS antennas, 10 antennas.

We also evaluate the performance of the WPCN with a larger number of WDs, $K = 5$, in Fig. 13. It is observed that the max-min rate decreases by increasing the number of WDs. This is because the common energy beamformer applied for all the WDs, should cover a larger number of WDs with different channel conditions. Another reason is that, the RIS which has a fixed number of antennas, needs to decode the received data from more WDs.

Fig. 14 demonstrates the max-min rate of the four EH models versus transmit power P_t at the PS for number of
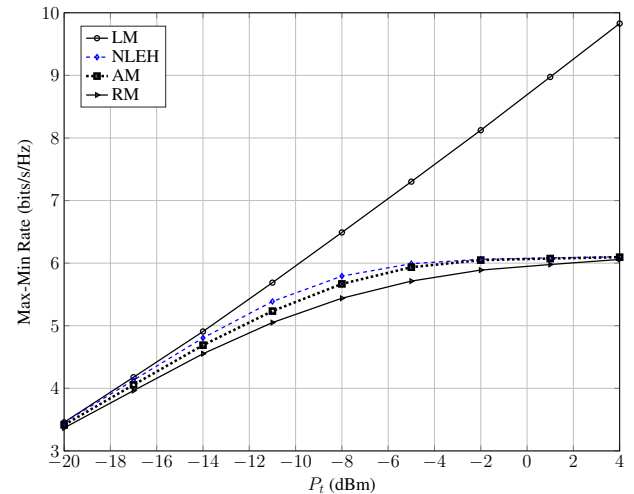

Fig. 14. Max-min rate versus P_t for $K = 3$, $N = 5$, $M = 7$ and $\eta = 0.6$.

WDs $K = 3$, number of PS antennas $N = 5$, number of IRS antennas $M = 7$ and power amplifier efficiency at WD $\eta = 0.6$. As expected, the max-min rate for the nonlinear EH models increases first and then converges to a plateau as P_t increases. Besides, among these models, LM offers the largest max-min rate, which indicates the overoptimistic nature of LM.

VIII. CONCLUSION

The linear EH model is the de facto standard for performance analysis and resource allocation of WPCNs. However, it fails to represent the saturation region of practical EH circuits. To overcome this issue, we proposed the new nonlinear EH model based on the error function. The model is described by three parameters, which can be determined by a best-fit search of an experiment data set. We also suggested the asymptotic model for the high transmit power regime, which consists of two parameters only. For comparative evaluation purposes, we also analyzed the linear as well as rational EH models.

To evaluate these models, we studied the average throughput of delay-limited and delay-tolerant transmission modes of the single-user network (Fig. 3) as well as average BER of BPSK and BDPSK. We also investigated the impact of large number of antennas at the PS and the impact of power control. Moreover, we investigated resource allocation for the multi-user WPCN to maximize the rate fairness under the proposed EH models. The results were validated via Monte-Carlo simulations and the four models were compared in Section VII.

Our main findings can be summarized as follows:
1) The newly proposed NLEH and AM models reach the saturation state, which coincides with the practical EH circuits character. The rational EH is also moderately accurate. However, the standard linear model is too optimistic in the high transmit power regime. Thus, its use for design and analysis purposes should be made with abundant caution.

2) The throughput and BER performances can be improved by increasing the number of antennas at the PS and/or at the IRS and by increasing the WD power amplifier efficiency. However, for nonlinear EH models, the performance saturation occurs for large transmit powers.

3) The performance of the WPCN significantly improves by designing the optimal beamformer in the WPT phase.

A. Future research topics

Our study of performance analysis and resource allocation for WPCNs with nonlinear/linear EH models points to several interesting future directions. Firstly, the new nonlinear and asymptotic EH models can be used to study simultaneous wireless information and power transfer (SWIPT) systems [66]. Secondly, these new models may also be extended for EH applications of secure cooperative communications networks, secrecy performance [7], resource allocations and full duplex systems [67] as well. Thirdly, our non-linear EH models may be studied over other propagation environments such as line-of-sight channels and Nakagami-m channels. These may arise particularly when the wireless power transfer takes place over short distances. Finally, the analytical formulas in this paper have been developed for the special case of $P_{se} = 0$. Thus, these may be generalized for non-zero sensitivity values.

APPENDIX A
GENERALIZED GAUSS–LAGUERRE QUADRATURE

When analyzing the performance of the network (Fig. 3), we find that the following integral must be computed often:

$$I = \int_0^\infty g(x) \frac{x^\alpha e^{-x}}{\Gamma(\alpha+1)} dx. \qquad (70)$$

Unfortunately, since $g(x)$ is a complicated function in most cases, a closed-form solution to (70) is elusive. Fortunately, the evaluation of (70) is extremely simple with numerical quadrature. Since the details of this method are not widely available, we briefly describe it herewith. It is based on the Gauss-Laguerre quadrature. The main idea is to use function $w(x) = x^\alpha e^{-x}$, $0 \le x < \infty$, to generate a set of orthogonal polynomials. Then, $g(x)$ in (70) is expressed as the weighted sum of these polynomials. Note that if $g(x)$ is a finite polynomial, then this expansion will be exact and error free. However, this is not the case in general. In any case, with this polynomial expansion, we can compute (70) as

$$I = \sum_{i=1}^n w_i g(x_i) + E_n, \qquad (71)$$

where E_n is an error term. The nodes $\{x_k\}$ are the roots of generalized Laguerre polynomials and weights $\{w_k\}$ are selected such that $E_n = 0$ if $g(x)$ is a polynomial of degree $\le n$ [68]. Of course, in our computations, $g(x)$ is not a polynomial, but it is a smooth function which can be approximated by a polynomial with sufficiently high degree. This means $E_n \to 0$ if we choose n large enough. Fortunately, the nodes x_k and weights w_k can be computed easily. This is

due to the fact that $\{x_k\}$ are the eigenvalues of the following, symmetric tridiagonal Jacobi matrix [69]:

$$J_n = \begin{bmatrix} u_0 & \sqrt{v_1} & & & & \\ \sqrt{v_1} & u_1 & \sqrt{v_2} & & & \\ & \sqrt{v_2} & \ddots & & \ddots & \\ & & & \ddots & u_{n-2} & \sqrt{v_{n-1}} \\ & & & & \sqrt{v_{n-1}} & u_{n-1} \end{bmatrix} \qquad (72)$$

where $u_k = 2k + \alpha + 1$ and $v_k = k(k+\alpha)$, $k = 0, \ldots n - 1$. Thus, the eigenvalues of this matrix and the formula (72) can be easily computed in any software environment such as MATLAB with only a few lines. For instance, we give the following MATLAB code:

```
function[x, w] = GaussLagurre(n, a)
% Generate nodes and weights for
% Gauss-Lagurre quadrature.
% w(x) = x ^a * e ^(-x)
u = (2 * (0 : n-1) + a + 1);
v= sqrt((1 : n - 1) .^2 + a * (1 : n-1));
[V, D] = eig(diag(u) + diag(v, 1)
+ diag(v, -1));
[x, i] = sort(diag(D));
Vtop = V(:, i)';
w = Vtop(:, 1).^2;
```

APPENDIX B
NECESSARY INTEGRAL

The following integral (73) frequently arises in the problems of ergodic capacity analysis and others. This integral has been derived in [70, Eq. (78)] as a summation of incomplete upper gamma function, which is more complicated than (74). For this reason, we give a proof below.

Lemma 1. *Let us consider*

$$I_n(u) = \int_0^\infty e^{-ux} x^n \log_2(1+x) dx, \qquad (73)$$

where $n \ge 0$ is a positive integer and $u > 0$. We can prove that

$$I_n(u) = \log_2(e) \left[e^u E_1(u) \sum_{k=0}^n \frac{n!(-1)^k}{k! u^{n-k+1}} \right.$$
$$\left. + \sum_{k=1}^n \sum_{l=1}^k \sum_{m=0}^{l-1} \frac{n!(-1)^{k+l}}{lm!(k-l)! u^{n-k+1-m+l}} \right], \qquad (74)$$

where $n!$ is the factorial and and $E_1(x) = \int_1^\infty \frac{e^{-xt}}{t} dt$ is the exponential integral function.

Proof. We note that

$$I_n(u) = (-1)^n \frac{d^n I_0(u)}{du^n} \qquad (75)$$

for $n = 0, 1, \ldots$.

It is easy to show that

$$I_0(u) = \log_2(e) \frac{e^u}{u} \underbrace{\int_1^\infty \frac{e^{-ut}}{t} dt}_{=E_1(u)}. \qquad (76)$$

The n-th derivative of $I_0(u)$ can be derived as follows:

$$
\begin{aligned}
\frac{d^n I_0(u)}{du^n} &\overset{(a)}{=} \log_2(e) \frac{d^n}{du^n}\left(\frac{e^u}{u}E_1(u)\right) \\
&\overset{(b)}{=} \log_2(e) \sum_{k=0}^{n}\binom{n}{k}\frac{d^{n-k}\left[u^{-1}\right]}{du^{n-k}}\frac{d^k\left[e^u E_1(u)\right]}{du^k} \\
&\overset{(c)}{=} \log_2(e) \sum_{k=0}^{n}\binom{n}{k}\frac{(-1)^{n-k}(n-k)!}{u^{n-k+1}}\frac{d^k\left[e^u E_1(u)\right]}{du^k} \\
&\overset{(d)}{=} \log_2(e) \sum_{k=0}^{n}\frac{n!(-1)^{n-k}}{k!u^{n-k+1}}\frac{d^k\left[e^u E_1(u)\right]}{du^k}.
\end{aligned}
\tag{77}
$$

The above steps are based upon the standard formula for the derivative of the product of two functions.

The k-th derivative of $e^u E_1(u)$ can be derived as follows:

$$
\begin{aligned}
\frac{d^k\left[e^u E_1(u)\right]}{du^k} &\overset{(a)}{=} \frac{d^k}{du^k}\left(e^u\int_1^\infty \frac{e^{-ut}}{t}dt\right) \\
&\overset{(b)}{=} \frac{d^k}{du^k}\left(\int_1^\infty \frac{e^{-u(t-1)}}{t}dt\right) \\
&\overset{(c)}{=} (-1)^k\int_1^\infty \frac{(t-1)^k e^{-u(t-1)}}{t}dt \\
&\overset{(d)}{=} (-1)^k\int_1^\infty \sum_{l=0}^{k}\binom{k}{l}t^l(-1)^{k-l}\frac{e^{-u(t-1)}}{t}dt \\
&\overset{(e)}{=} \left[e^u E_1(u)+\int_1^\infty\sum_{l=1}^{k}\binom{k}{l}t^l(-1)^l\frac{e^{-u(t-1)}}{t}dt\right] \\
&\overset{(f)}{=} \left[e^u E_1(u)+\int_1^\infty\sum_{l=1}^{k}\binom{k}{l}t^{l-1}(-1)^l e^{-u(t-1)}dt\right] \\
&\overset{(g)}{=} \left[e^u E_1(u)+\int_0^\infty\sum_{l=1}^{k}\binom{k}{l}(t+1)^{l-1}(-1)^l e^{-ut}dt\right] \\
&\overset{(h)}{=} \left[e^u E_1(u)+\int_0^\infty(-1)^l\sum_{l=1}^{k}\sum_{m=0}^{l-1}\binom{k}{l}\binom{l-1}{m}t^{l-1-m}e^{-ut}dt\right] \\
&\overset{(i)}{=} \left[e^u E_1(u)+(-1)^l\sum_{l=1}^{k}\sum_{m=0}^{l-1}\binom{k}{l}\binom{l-1}{m}\frac{(l-m-1)!}{u^{l-m}}\right].
\end{aligned}
\tag{78}
$$

Since the above steps are self-explanatory, we omit the details. By substituting (78) in (77) and after some manipulations, we obtain (74). ∎

APPENDIX C
PROOF OF PROPOSITION 1

Since the received signal power at the IRS is random, it is possible that the SNR may drop below the required threshold, resulting in an outage. Thus, OP is defined as

$$
P_{out} = \Pr\left(\gamma < \gamma_{\text{th}}\right) = \Pr\left(||\mathbf{g}||^2 < \frac{\gamma_{\text{th}}}{cP_h}\right),
\tag{79}
$$

where $\gamma_{\text{th}} = 2^R - 1$ is a predetermined threshold.

In order to evaluate (79), we first average over $||\mathbf{g}||^2$ while keeping P_h constant:

$$
\begin{aligned}
P_{out}\mid_{P_h} &= \int_0^{\frac{\gamma_{\text{th}}}{cP_h}}\frac{1}{\Gamma(M)}y^{M-1}e^{-y}dy \\
&\overset{(a)}{=} \frac{1}{\Gamma(M)}\gamma\left(M,\frac{\gamma_{\text{th}}}{cP_h}\right),
\end{aligned}
\tag{80}
$$

where the above follows from the fact that $||\mathbf{g}||^2$ is Gamma distributed and the incomplete Gamma function is given by [44, Eq. (5.531.1)].

Second, since P_h is a function of $||\mathbf{h}||^2$, we must average the conditional outage (80) over the PDF of $||\mathbf{h}||^2$. This can be done as follows

$$
\begin{aligned}
P_{out} &= \int_0^\infty P_{out}\mid_{P_h} f_{||\mathbf{h}||^2}(x)\,dx \\
&= \frac{1}{\Gamma(N)\Gamma(M)}\int_0^\infty \gamma\left(M,\frac{\gamma_{\text{th}}}{cq\left(\bar{P}_t x\right)}\right)x^{N-1}e^{-x}dx.
\end{aligned}
\tag{81}
$$

Finally, inserting (81) into (13), the average throughput of delay-limited mode can be expressed as (14).

APPENDIX D
PROOF OF PROPOSITION 2

Starting from the definition of the EC, we have

$$
\begin{aligned}
C_e &= \mathbb{E}\left[\log_2\left(1+cP_h||\mathbf{g}||^2\right)\right] \\
&\overset{(a)}{=} \mathbb{E}\left[\frac{1}{\Gamma(M)}\int_0^\infty \log_2\left(1+cP_h y\right)y^{M-1}e^{-y}dy\right] \\
&\overset{(b)}{=} \mathbb{E}\left[\frac{1}{\Gamma(M)}\left(cP_h\right)^{-M}\int_0^\infty \log_2\left(1+x\right)x^{M-1}e^{-\frac{x}{cP_h}}dx\right] \\
&\overset{(c)}{=} \mathbb{E}\left[\frac{\left(cP_h\right)^{-M}}{\Gamma(M)}I_{M-1}\left(\frac{1}{cP_h}\right)\right] \\
&\overset{(d)}{=} \frac{1}{\Gamma(N)\Gamma(M)}\int_0^\infty I_{M-1}\left(\frac{1}{cq\left(\bar{P}_t x\right)}\right)\frac{x^{N-1}e^{-x}}{\left(cq\left(\bar{P}_t x\right)\right)^M}dx,
\end{aligned}
\tag{82}
$$

where Step (a) is obtained by substituting the PDF of $||\mathbf{g}||^2$ into the definition of ergodic capacity; Let $x = cP_h y$ we obtain Step (b); Step (c) follows the Lemma 1; (d) is due to averaging (c) over $||\mathbf{h}||^2$.

APPENDIX E
PROOF OF PROPOSITION 3

The average BER of BPSK for a communication link that has a single antenna transmitter and multiple receive antennas with maximal ratio combining has been studied in [71, Section(14.4)]. The received SNR in this system is given by $\gamma = c||\mathbf{g}||^2$. This system is thus comparable to our WD-IRS link in Fig. 4, if P_h is assumed to be constant. Using this analysis, we find

$$
\begin{aligned}
\bar{P}_{BER} &= \mathbb{E}\left[Q\left(\sqrt{2cP_h||\mathbf{g}||^2}\right)\right] \\
&\overset{(a)}{=} \mathbb{E}\left[\left[\frac{1}{2}\left(1-\eta_1\right)\right]^M\sum_{k=0}^{M-1}\binom{M-1+k}{k}\left[\frac{1}{2}\left(1+\eta_1\right)\right]^k\right],
\end{aligned}
\tag{83}
$$

where $\eta_1 = \sqrt{\frac{cq(\bar{P}_t||\mathbf{h}||^2)}{1+cq(\bar{P}_t||\mathbf{h}||^2)}}$ and the Gaussian Q-function is given by $Q(x) = \frac{1}{\sqrt{2\pi}} \int_x^\infty e^{-t^2/2}dt = \frac{1}{2\sqrt{\pi}}\Gamma\left(\frac{1}{2}, \frac{x^2}{2}\right)$. Step (a) above is obtained by [71, Eq. (14.4.15)]. Averaging over $||\mathbf{h}||^2$, we have (17).

APPENDIX F
PROOF OF PROPOSITION 4

The conditional BER of BDPSK can be expressed as $P_c(x) = \frac{1}{2}e^{-x}$. Thus, the average BER is related to the MGF method [49]. Since by definition MGF of X is the expected value of random variable e^{tX}, where for the problem at hand X is the received SNR at the IRS, we first derive the MGF of it as

$$
\begin{aligned}
M(t) &= \mathbb{E}\left[e^{-cP_h||\mathbf{g}||^2 t}\right] \\
&\overset{(a)}{=} \mathbb{E}\left[\frac{1}{1 + ctq\left(P_t||\mathbf{h}||^2\right)}\right]^M \\
&\overset{(b)}{=} \frac{1}{\Gamma(N)} \int_0^\infty \frac{x^{N-1}e^{-x}}{\left[1 + ctq\left(P_t x\right)\right]^M} dx,
\end{aligned}
\tag{84}
$$

where (a) is obtained by taking the expectation over the distribution of $||\mathbf{g}||^2$, which is Gamma distributed and thus follows from and then averaging over $||\mathbf{h}||^2$, we can have (b).

Thus, the average BER of BDPSK can be obtained via (84), which results in (18).

REFERENCES

[1] Cisco, "Cisco annual report 2018-2023." https://www.cisco.com/c/en/us/solutions/collateral/executive-perspectives/annual-internet-report/white-paper-c11-741490.html, 2020.

[2] C. Bockelmann, N. Pratas, H. Nikopour, K. Au, T. Svensson, C. Stefanovic, P. Popovski, and A. Dekorsy, "Massive machine-type communications in 5G: Physical and MAC-layer solutions," *IEEE Commun. Mag*, vol. 54, pp. 59–65, Sep. 2016.

[3] Z. Ding, C. Zhong, D. W. K. Ng, M. Peng, H. A. Suraweera, R. Schober, and H. V. Poor, "Application of smart antenna technologies in simultaneous wireless information and power transfer," *IEEE Commun. Mag*, vol. 53, pp. 86–93, Apr. 2015.

[4] Powercast, "The product of powercast." https://www.powercastco.com/our-products/, 2020.

[5] M.-L. Ku, W. Li, Y. Chen, and K. R. Liu, "Advances in energy harvesting communications: Past, present, and future challenges," *IEEE Commun. Surveys Tuts*, vol. 18, pp. 1384–1412, Nov. 2015.

[6] H. Ju and R. Zhang, "Throughput maximization in wireless powered communication networks," *IEEE Trans. Wireless Commun.*, vol. 13, pp. 418–428, Dec. 2013.

[7] Z. Mobini, M. Mohammadi, and C. Tellambura, "Wireless-powered full-duplex relay and friendly jamming for secure cooperative communications," *IEEE Trans. Inf. Forensics Security*, vol. 14, pp. 621–634, Jul. 2018.

[8] B. Lyu, T. Qi, H. Guo, and Z. Yang, "Throughput maximization in full-duplex dual-hop wireless powered communication networks," *IEEE Access*, vol. 7, pp. 158584–158593, Oct. 2019.

[9] C. Guo, B. Liao, L. Huang, Q. Li, and X. Lin, "Convexity of fairness-aware resource allocation in wireless powered communication networks," *IEEE Commun. Lett.*, vol. 20, pp. 474–477, Jan. 2016.

[10] L. Liu, R. Zhang, and K.-C. Chua, "Multi-antenna wireless powered communication with energy beamforming," *IEEE Trans. Commun.*, vol. 62, pp. 4349–4361, Dec. 2014.

[11] F. Zhao, H. Lin, C. Zhong, Z. Hadzi-Velkov, G. K. Karagiannidis, and Z. Zhang, "On the capacity of wireless powered communication systems over Rician fading channels," *IEEE Trans. Commun.*, vol. 66, pp. 404–417, Sep. 2017.

[12] D. Altinel and G. K. Kurt, "Energy harvesting from multiple RF sources in wireless fading channels," *IEEE Trans. Veh. Technol.*, vol. 65, pp. 8854–8864, Jan. 2016.

[13] H. Gonçalves, M. Martins, and J. Fernandes, "Fully integrated energy harvesting circuit with- 25-dBm sensitivity using transformer matching," *IEEE Trans. Circuits Syst. II*, vol. 62, pp. 446–450, Jan. 2015.

[14] Y. Chen, N. Zhao, and M.-S. Alouini, "Wireless energy harvesting using signals from multiple fading channels," *IEEE Trans. Commun.*, vol. 65, pp. 5027–5039, Nov. 2017.

[15] W. Huang, H. Chen, Y. Li, and B. Vucetic, "On the performance of multi-antenna wireless-powered communications with energy beamforming," *IEEE Trans. Veh. Technol.*, vol. 65, pp. 1801–1808, Mar. 2016.

[16] Y. Ma, H. Chen, Z. Lin, Y. Li, and B. Vucetic, "Distributed and optimal resource allocation for power beacon-assisted wireless-powered communications," *IEEE Trans. Commun.*, vol. 63, pp. 3569–3583, Oct. 2015.

[17] G. Pan, H. Lei, and Y. Deng, "On secrecy performance of MISO SWIPT systems with TAS and imperfect CSI," *IEEE Trans. Commun.*, vol. 64, pp. 3831–3843, Sep. 2016.

[18] Y. Liu, "Wireless information and power transfer for multirelay-assisted cooperative communication," *IEEE Communications Letters*, vol. 20, pp. 784–787, Apr. 2016.

[19] D. Khan, S. J. Oh, K. Shehzad, M. Basim, D. Verma, Y. G. Pu, M. Lee, K. C. Hwang, Y. Yang, and K. Lee, "An efficient reconfigurable RF-DC converter with wide input power range for RF energy harvesting," *IEEE Access*, vol. 8, pp. 79310–79318, May 2020.

[20] Z. Hameed and K. Moez, "Hybrid forward and backward threshold-compensated RF-DC power converter for RF energy harvesting," *IEEE Trans. Emerg. Sel. Topics Circuits Syst.*, vol. 4, pp. 335–343, Sep. 2014.

[21] T. Le, K. Mayaram, and T. Fiez, "Efficient far-field radio frequency energy harvesting for passively powered sensor networks," *IEEE J. Solid-State Circuits*, vol. 43, pp. 1287–1302, May 2008.

[22] S. Ladan and K. Wu, "Nonlinear modeling and harmonic recycling of millimeter-wave rectifier circuit," *IEEE Trans. Microw. Theory Techn.*, vol. 63, pp. 937–944, Mar. 2015.

[23] J. Guo and X. Zhu, "An improved analytical model for RF-DC conversion efficiency in microwave rectifiers," in *Proc. IEEE MTT-S Int. Microw. Symp. Dig.*, pp. 1–3, IEEE, Aug. 2012.

[24] S. Pejoski, Z. Hadzi-Velkov, and R. Schober, "Optimal power and time allocation for WPCNs with piece-wise linear EH model," *IEEE Commun. Lett.*, vol. 7, pp. 364–367, Jun. 2017.

[25] K. Xiong, B. Wang, and K. R. Liu, "Rate-energy region of SWIPT for MIMO broadcasting under nonlinear energy harvesting model," *IEEE Trans. Wireless Commun.*, vol. 16, pp. 5147–5161, Aug. 2017.

[26] H. Lyu, X. Liu, Y. Sun, Z. Jian, and A. Babakhani, "A 915-MHz far-field energy harvester with- 22-dBm sensitivity and 3-V output voltage based on antenna-and-rectifier codesign," *IEEE Microw. Wireless Compon. Lett.*, vol. 29, pp. 557–559, Aug. 2019.

[27] Y. Chen, *Energy Harvesting Communications: Principles and Theories*. John Wiley & Sons, 2019.

[28] Y. Dong, M. J. Hossain, and J. Cheng, "Performance of wireless powered amplify and forward relaying over Nakagami-m fading channels with nonlinear energy harvester," *IEEE Commun. Lett.*, vol. 20, pp. 672–675, Apr. 2016.

[29] Y. Chen, K. T. Sabnis, and R. A. Abd-Alhameed, "New formula for conversion efficiency of RF EH and its wireless applications," *IEEE Trans. Veh. Technol.*, vol. 65, pp. 9410–9414, Nov. 2016.

[30] B. Clerckx and E. Bayguzina, "Waveform design for wireless power transfer," *IEEE Trans. Signal Process.*, vol. 64, pp. 6313–6328, Dec. 2016.

[31] E. Boshkovska, D. W. K. Ng, N. Zlatanov, and R. Schober, "Practical non-linear energy harvesting model and resource allocation for SWIPT systems," *IEEE Commun. Lett.*, vol. 19, pp. 2082–2085, Dec. 2015.

[32] S. Wang, M. Xia, K. Huang, and Y.-C. Wu, "Wirelessly powered two-way communication with nonlinear energy harvesting model: Rate regions under fixed and mobile relay," *IEEE Trans. Wireless Commun.*, vol. 16, pp. 8190–8204, Dec. 2017.

[33] J. Zhang and G. Pan, "Outage analysis of wireless-powered relaying MIMO systems with non-linear energy harvesters and imperfect CSI," *IEEE Access*, vol. 4, pp. 7046–7053, Nov. 2016.

[34] R. Jiang, K. Xiong, P. Fan, L. Zhou, and Z. Zhong, "Outage probability and throughput of multirelay SWIPT-WPCN networks with nonlinear EH model and imperfect CSI," *IEEE Syst. J.*, vol. 14, pp. 1206–1217, Mar. 2020.

[35] J. Zhang, G. Pan, and Y. Xie, "Secrecy analysis of wireless-powered multi-antenna relaying system with nonlinear energy harvesters and imperfect CSI," *IEEE Trans. Green Commun. Netw.*, vol. 2, pp. 460–470, Jun. 2017.

[36] Y. Huang, T. Q. Duong, J. Wang, and P. Zhang, "Performance of multi-antenna wireless-powered communications with nonlinear energy harvester," in *IEEE 86th Vehicular Technology Conference (VTC-Fall)*, pp. 1–6, 2017.

[37] Y. Wang, Y. Wu, F. Zhou, Z. Chu, Y. Wu, and F. Yuan, "Multi-objective resource allocation in a NOMA cognitive radio network with a practical non-linear energy harvesting model," *IEEE Access*, vol. 6, pp. 12973–12982, Mar. 2017.

[38] Y. Wang, Y. Wang, F. Zhou, Y. Wu, and H. Zhou, "Resource allocation in wireless powered cognitive radio networks based on a practical non-linear energy harvesting model," *IEEE Access*, vol. 5, pp. 17618–17626, Sep. 2017.

[39] R. Morsi, E. Boshkovska, E. Ramadan, D. W. K. Ng, and R. Schober, "On the performance of wireless powered communication with non-linear energy harvesting," in *Proc. IEEE 18th Int. Workshop Signal Process. Adv. Wireless Commun. (SPAWC)*, pp. 1–5, IEEE, Jul. 2017.

[40] L. Cantos and Y. H. Kim, "Max-min fair energy beamforming for wireless powered communication with non-linear energy harvesting," *IEEE Access*, vol. 7, pp. 69516–69523, Jun. 2019.

[41] X. Zhang, Y. Wang, F. Zhou, N. Al-Dhahir, and X. Deng, "Robust resource allocation for MISO cognitive radio networks under two practical non-linear energy harvesting models," *IEEE Commun. Lett.*, vol. 22, no. 9, pp. 1874–1877, 2018.

[42] E. Boshkovska, D. W. K. Ng, N. Zlatanov, A. Koelpin, and R. Schober, "Robust resource allocation for MIMO wireless powered communication networks based on a non-linear EH model," *IEEE Trans. Commun.*, vol. 65, pp. 1984–1999, Dec. 2017.

[43] M. Stoopman, S. Keyrouz, H. Visser, K. Philips, and W. Serdijn, "A self-calibrating RF energy harvester generating 1V at -26.3 dBm," in *Proc. IEEE Symposium on VLSI Circuits (VLSIC)*, pp. 226–227, IEEE, Jun. 2013.

[44] I. S. Gradshteyn and I. M. Ryzhik, *Table of Integrals, Series, and Products, 7th edition*. Academic Press, 2007.

[45] X. Chen, C. Yuen, and Z. Zhang, "Wireless energy and information transfer tradeoff for limited-feedback multiantenna systems with energy beamforming," *IEEE Trans. Veh. Technol.*, vol. 63, pp. 407–412, Jan. 2013.

[46] M. Taghadosi, L. Albasha, N. A. Quadir, Y. A. Rahama, and N. Qaddoumi, "High efficiency energy harvesters in 65nm CMOS process for autonomous IoT sensor applications," *IEEE Access*, vol. 6, pp. 2397–2409, Dec. 2017.

[47] Z. Chang, S. Zhang, and Z. Wang, "Energy efficient optimisation for large-scale multiple-antenna system with WPT," *IET Commun.*, vol. 12, pp. 552–558, Feb. 2018.

[48] C. Tellamura, A. Annamalai, and V. Bhargava, "Closed form and infinite series solutions for the MGF of a dual-diversity selection combiner output in bivariate Nakagami fading," *IEEE Trans. Commun.*, vol. 51, pp. 539–542, Apr. 2003.

[49] C. Tellambura, "Evaluation of the exact union bound for trellis-coded modulations over fading channels," *IEEE Trans. Commun.*, vol. 44, pp. 1693–1699, Dec. 1996.

[50] W. Zhao, G. Wang, S. Atapattu, C. Tellambura, and H. Guan, "Outage analysis of ambient backscatter communication systems," *IEEE Commun. Lett.*, vol. 22, pp. 1736–1739, Aug. 2018.

[51] IEEE, "IEEE 802.15.4." "http://www.ieee802.org/15/pub/TG4.html.".

[52] IEEE, "IEEE 802.11-1999." https://standards.ieee.org/standard/802.11-1999.html.

[53] H. Lei, J. Zhang, K.-H. Park, P. Xu, Z. Zhang, G. Pan, and M.-S. Alouini, "Secrecy outage of max–min TAS scheme in MIMO-NOMA systems," *IEEE Trans. Veh. Technol.*, vol. 67, pp. 6981–6990, Aug. 2018.

[54] F. Rezaei, C. Tellambura, A. Tadaion, and A. R. Heidarpour, "Rate analysis of cell-free massive MIMO-NOMA with three linear precoders," *IEEE Trans. Commun.*, Jun. 2020.

[55] C. Zhang, Y. Jing, Y. Huang, and L. Yang, "Performance scaling law for multicell multiuser massive MIMO," *IEEE Trans. Veh. Technol.*, vol. 66, pp. 9890–9903, Nov. 2017.

[56] S. Silva, G. A. A. Baduge, M. Ardakani, and C. Tellambura, "Performance analysis of massive MIMO two-way relay networks with pilot contamination, imperfect CSI, and antenna correlation," *IEEE Trans. Veh. Technol.*, vol. 67, pp. 4831–4842, Jun. 2018.

[57] G. Sacarelo, I. Song, and Y. H. Kim, "Beamforming and resource allocation for a multi-pair wireless powered two-way relay network with fairness," *IEEE Access*, vol. 7, pp. 2799–2810, Dec. 2019.

[58] M. Razaviyayn, *Successive convex approximation: Analysis and applications*. Ph.D. dissertation, Univ. Minnesota, Minneapolis, MN, USA, 2014.

[59] L. Tran, M. F. Hanif, and M. Juntti, "A conic quadratic programming approach to physical layer multicasting for large-scale antenna arrays," *IEEE Signal Process. Lett.*, vol. 21, pp. 114–117, Jan. 2014.

[60] N. D. Sidiropoulos, T. N. Davidson, and Zhi-Quan Luo, "Transmit beamforming for physical-layer multicasting," *IEEE Trans. Signal Process.*, vol. 54, pp. 2239–2251, Jun. 2006.

[61] V.-B. Nguyen, R.-L. Sheu, and Y. Xia, "An SDP approach for solving quadratic fractional programming problems," *arXiv preprint arXiv:1402.4198*, Mar. 2014.

[62] J.-P. Crouzeix and J. A. Ferland, "Algorithms for generalized fractional programming," *Mathematical Programming*, vol. 52, pp. 191–207, May 1991.

[63] S. Boyd and L. Vandenberghe, *Convex Optimization*. Cambridge, U.K.: Cambridge Univ. Press, 2004.

[64] G. Yang, C. K. Ho, R. Zhang, and Y. L. Guan, "Throughput optimization for massive MIMO systems powered by wireless energy transfer," *IEEE J. Sel. Area. Comm.*, vol. 33, pp. 1640–1650, Aug. 2015.

[65] "Powercast corp. product datasheet, P2110-915MHz RF power harvester." http://www.econ.ucsb.edu/~tedb/Theory/delta.pdf.

[66] G. Pan, H. Lei, Y. Yuan, and Z. Ding, "Performance analysis and optimization for SWIPT wireless sensor networks," *IEEE Trans. Commun.*, vol. 65, pp. 2291–2302, May 2017.

[67] M. Mohammadi, H. A. Suraweera, Y. Cao, I. Krikidis, and C. Tellambura, "Full-duplex radio for uplink/downlink wireless access with spatially random nodes," *IEEE Trans. Commun.*, vol. 63, pp. 5250–5266, Dec. 2015.

[68] W. Gautschi, *Orthogonal Polynomials*. Oxford university press Oxford, 2004.

[69] J. A. Gubner, "A new formula for lognormal characteristic functions," *IEEE Trans. Veh. Technol.*, vol. 55, pp. 1668–1671, Sep. 2006.

[70] M.-S. Alouini and A. J. Goldsmith, "Capacity of Rayleigh fading channels under different adaptive transmission and diversity-combining techniques," *IEEE Trans. Veh. Technol.*, vol. 48, pp. 1165–1181, Jun. 1999.

[71] J. G. Proakis and M. Salehi, *Digital Communications*, vol. 4. McGraw-hill New York, 2001.